VENTRAL ROOT OR DORSAL ROOT GANGLION MICROSTIMULATION TO EVOKE HINDLIMB MOTOR RESPONSES

by

Dennis Joseph Bourbeau

BS, Worcester Polytechnic Institute, 2002

Submitted to the Graduate Faculty of

the Swanson School of Engineering in partial fulfillment

of the requirements for the degree of

Doctor of Philosophy

University of Pittsburgh

2011

UNIVERSITY OF PITTSBURGH

SWANSON SCHOOL OF ENGINEERING

This dissertation was presented

by

Dennis Joseph Bourbeau

It was defended on

June 22, 2011

and approved by

Xinyan Tracy Cui, Ph.D., Associate Professor, Department of Bioengineering

H. Richard Koerber, Ph.D., Professor, Department of Neurobiology

Jonathan E. Rubin, Ph.D., Professor, Department of Mathematics

Dissertation Director: Douglas J. Weber, Ph.D., Assistant Professor, Departments of Bioengineering and Physical Medicine and Rehabilitation, UPMC

VENTRAL ROOT OR DORSAL ROOT GANGLION MICROSTIMULATION TO EVOKE HINDLIMB MOTOR RESPONSES

Dennis Joseph Bourbeau, PhD

University of Pittsburgh, 2011

Functional electrical stimulation is an important therapeutic tool for improving the quality of life of patients following spinal cord injury. Investigators have developed neural interfaces of varying invasiveness and implant location to stimulate neurons and evoke motor responses. Here we present an alternative interface with the ventral roots (VR) or dorsal root ganglia (DRG). We designed preliminary electrophysiology experiments to evaluate the performance of these interfaces, wherein we stimulated lumbar VR or DRG through a penetrating single-wire microelectrode while recording fixed endpoint force and bipolar electromyograms of hindlimb muscles. Data from rat experiments provided evidence for selectivity for target muscles, graded force recruitment, and nontrivial force magnitudes of up to 1 N. Electrophysiology experiments in cats produced similar results to those in rats. In addition, we developed a computational model to estimate the size and quantity of fibers recruited as a function of stimulus amplitude. This model confirmed electrophysiology results showing differences in the thresholds to detect activity in response to VR versus DRG stimulation. The model also provided insights into the mechanisms by which DRG stimulation is more likely to recruit smaller fibers than larger fibers. Finally, we discuss further work to develop and evaluate these potential interfaces.

TABLE OF CONTENTS

LIST OF TABLES

LIST OF FIGURES

PREFACE

Thank you for taking the time to read this preface. Allow me to begin by offering a very special and personal "Welcome" from me, Dennis Bourbeau, to you. And that's not just any "Welcome"; it comes with a smile and a figurative handshake, with a firm grip mind you. In today's fast-paced world, we often feel the need to skim, focusing on those bits that are most relevant. But you, courageous reader, considerate reader, curious reader, chose to take this time from what is undoubtedly a hectic schedule. If you'd like to pause a moment, perhaps nip off for a snack or some coffee, maybe make an important telephone call, we can wait. I like to think that what follows will be a challenging but fruitful discussion of some of my graduate work. And if you enjoy this document half as much as I enjoyed writing it, then I shall have enjoyed it twice as much as you. But first, I have some important announcements.

It is commonly known that I dislike acronyms and prefer to avoid them when possible. However, in writing this dissertation, I have made liberal use of a few acronyms that are common in the literature. These acronyms are as follows: FES – functional electrical stimulation; VR – ventral root; DRG – dorsal root ganglion; IFMS – intrafascicular microstimulation; and ISMS – intraspinal microstimulation. These acronyms are also defined in the body of this document when they are introduced.

Penultimately, I would like to acknowledge some of those people who need acknowledging. Ingrid Albrecht, Erika Rost and Tyler Simpson provided important assistance with surgeries, histology, and technical assistance on a number of fronts. My colleagues in Doug

Weber's lab graciously offered feedback on my ideas, presentations, and writing, with a minimum of eye-rolling or face-palming. They encouraged me, challenged me, criticized me and were handsome people with whom to work.

Finally, to my wife, Catherine, and my children, Remy and Gabrielle: you consistently offered your love and support. You have helped me keep my motivation and perspective, while mercifully preventing me from taking myself too seriously.

Dear reader, kind reader, thank you for indulging me. Let us get on with it.

1.0 INTRODUCTION

1.1 PARALYSIS AND RESULTING LOSS OF MOTOR FUNCTION

In 2010, approximately 12,000 Americans survived a spinal cord injury [1] and approximately 645,000 survived a stroke [2]. These two causes account for approximately 52% of the almost 6 million patients currently suffering paralysis in the United States [3]. Not only must these patients adapt to a new quality of life because of a decrease in or loss of motor function, they must also learn to manage a number of complications associated with paralysis. These complications include obesity, hypertension, abnormal lipid profiles, pressure sores and muscle atrophy, among others [4, 5]. In spinal cord injury cases, increased rates of thrombosis are reported, which lead to diminished arterial circulation in both blood flow volume and velocity [6]. Because blood supply is diminished, secondary complications result, including decreased oxygenation of paralyzed tissues, slower healing of cutaneous injuries and increased incidents of pressure sores [7].

Emphasis has been placed on technologies that improve patient independence and diminish complications through increased mobility. One approach has been the targeted application of small electrical currents to activate motor fibers and thus evoke controlled muscle contractions for restoring motor function. As early as 1961, Liberson and colleagues [8] described stimulation of the peroneal nerve during swing phase of human gait in order to treat

foot drop. In 1962, Moe and Post used the term "functional electrical stimulation" (FES) to describe this technique for improving ambulation in hemiplegic patients [9]. Researchers and clinicians have since developed FES as a therapeutic intervention for persons with loss of motor function due to paralysis. Studies have shown that exercise derived from the use of lower limb FES systems has measurable benefits on the health of spinal cord-injured (SCI) patients, such as preventing muscle atrophy [10], decreasing the risk of pressure sores [11], increasing vasculature, improving circulation [12], and reducing depression [13]. These results are not unexpected because the benefits of exercise have already been shown in the general population. Most importantly, FES systems have been able to introduce an improved level of patient independence through the ability to stand and walk [14].

1.2 APPROACHES TO RESTORING MOTOR FUNCTION

The focus of this dissertation is the design of the physical interface between the biological tissue and the medical device providing electrical stimulation to elicit motor responses. Several approaches have been developed to deliver electrical stimulation and evoke controlled contractions of skeletal muscles for an FES system. Each interface type has its strengths and weaknesses with respect to their performance in FES systems. These approaches include surface, epimysial, intramuscular, extraneural, intraneural and intraspinal electrode interfaces [15]. Surface stimulation is attractive because it is non-invasive (Figure 1.1A). Electrodes are applied to the skin and placement is unique for each patient. With this interface, stimulation is designed to activate a whole nerve innervating a target muscle or muscles. FES systems incorporating surface stimulation include the WalkAide (Innovate Neurotronics, Inc.) and NESS L300

(Bioness, Inc.) systems for correcting foot drop, the Parastep system (Sigmedics, Inc.) for standing and walking, and the NESS H200 (Bioness, Inc.) system for restoring handgrip.

Epimysial electrodes are implanted on the surface of a muscle, just under the skin. Intramuscular electrodes, however, are implanted *into* the muscle. Extraneural electrodes, such as nerve cuffs, offer some improvements over less invasive interfaces (Figure 1.1B). These electrodes wrap around the nerve and stimulation is designed to activate fibers within a target fascicle, where the efferents within a fascicle innervate the same muscle group. Nerve cuffs have notably been used in devices for correcting foot drop, such as the Stimustep (Finetech Medical Ltd.) and the ActiGait (Neurodan A/S) systems.

Intraneural electrodes have been developed that interface with a small population of neuronal fibers. Intrafascicular stimulation (IFMS), for example, is designed to activate a group of fibers within a peripheral nerve fascicle (Figure 1.1C). Finally, intraspinal microstimulation (ISMS) has been tested as a means of restoring motor function (Figure 1.1D). With this interface, electrodes are implanted into the ventral laminae of the spinal cord. The strategy when using ISMS is to activate some of the spinal circuitry to produce complex movements, including movement primitives for generating locomotion [16].

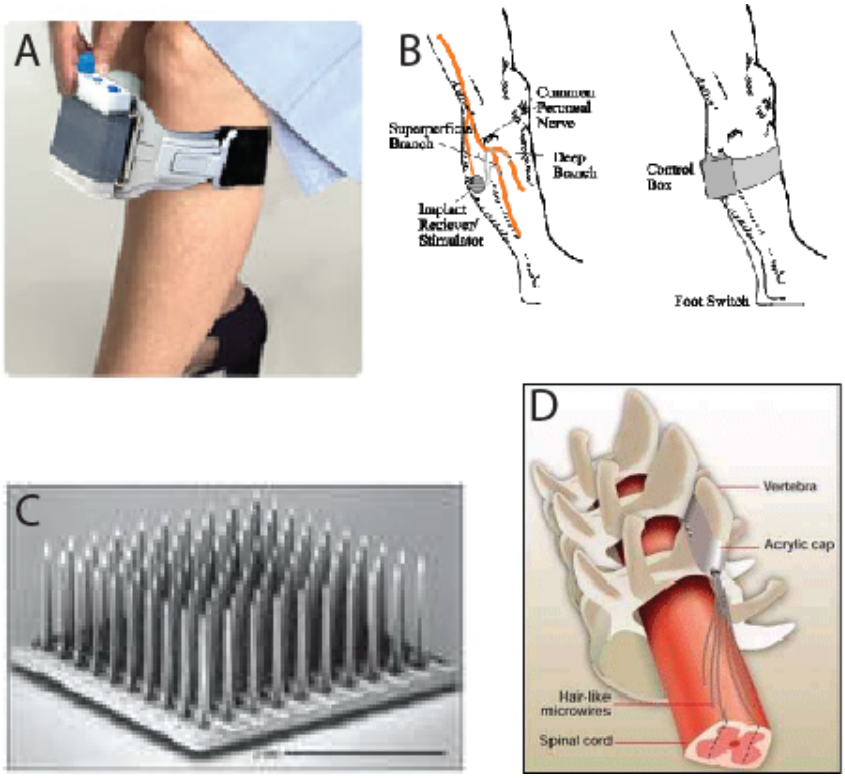

Figure 1.1 Examples of existing FES interfaces. (A) The WalkAide is a clinically available device that uses a surface electrode interface to correct foot drop (www.walkaide.com). (B) The STIMuSTEP, also for correcting foot drop, uses an implanted nerve cuff to stimulate the peroneal nerve directly (www.salisburyfes.com). (C) Intrafascicular electrodes penetrate the epineurium to access the fascicles within a peripheral nerve (www.blackrockmicro.com). This interface takes advantage of multiple electrode sites, usually designed as a microelectrode array. (D) Intraspinal microstimulation involves implanting microwires into the ventral laminae of the spinal cord to access motor pools (www.ualberta.ca/~aprochaz).

1.3 CAPABILITIES AND LIMITATIONS OF EXISTING INTERFACES

An ideal FES system allows the user to make graceful, dexterous movements with sufficient force and stamina to complete motor tasks. The user should also be able to carefully control the amount of force applied to these tasks. To meet these objectives, we take into account a number of design criteria when developing an interface for an FES system, including

selectivity, fatigue resistance, force recruitment, and power consumption. The interface should provide selective access to target muscles, allowing for activation of a target muscle without spillover into its mutual antagonist, and therefore avoiding co-contractions. In addition, repeatedly stimulating the same neurons may result in fatigue before completion of an extended motor task, such as walking, but sufficient access to discrete populations of neurons innervating a target muscle can provide an opportunity to stimulate those populations alternatingly and thus resist fatigue. We define force recruitment as the amount of force generated as a function of stimulus parameters, such as stimulus intensity. To achieve controlled, graceful movements, stimulation should produce graded rather than steep increases in force magnitude as stimulus intensity is increased. Moreover, stimulation through the interface should result in functional force magnitudes, large enough to complete a motor task. Finally, power consumption is a function both of the number of stimulus channels and the stimulus charge required to evoke a motor response per stimulus channel. While increasing the number of channels may increase our selectivity, we wish to simultaneously use less charge per channel. These are some of the important metrics to consider when evaluating the design of an FES interface. Table 1.1 summarizes a qualitative comparison of existing interfaces by these metrics.

While surface stimulation is the least invasive interface, there are several drawbacks, which include the need for daily placement of the electrodes and frequent recalibration. Because these devices lack the ability to finely control current spread, thus limiting selectivity, surface stimulation is most suitable for applications involving whole activation of a peripheral nerve, such as the peroneal nerve to treat foot drop. Epimysial and intramuscular electrodes are slightly more invasive, but allow for stimulation targeting a particular muscle, thus improving selectivity over surface electrodes. Hughes and colleagues demonstrated that multiple epimysial electrodes

per muscle could be used for interleaved stimulation, which delayed onset of fatigue and reduced ripple in the muscle contractile force [17]. In addition, Singh and colleagues concluded that intramuscular stimulation produced more graded recruitment of force with less fatigue than stimulation with nerve cuffs [18]. However, spillover is a problem with these systems, as non-target muscles are inadvertently stimulated along with target muscles [19]. Moreover, these electrodes do not necessarily achieve complete activation of the target muscles and the stimulus thresholds are ten-fold higher compared to electrodes that stimulate the nerves directly [20].

The advantage to using a nerve cuff electrode instead of a surface electrode is that there is more complete activation of the peroneal nerve for achieving dorsiflexion and placement of the electrode is simplified. Improvements are being made to extraneural interfaces. The flat interface nerve electrode (FINE) is a modified nerve cuff, which reshapes the nerve, flattening it in an attempt to spread out and line up the fascicles for better fascicular selectivity [21]. Current steering using specialized electrode configurations can also improve fascicle selectivity [22, 23]. Nonetheless, extraneural stimulation remains limited in its ability to achieve fatigue-resistance, graded force recruitment, and selectivity for fibers within a nerve fascicle in comparison to intrafascicular interfaces.

IFMS has three important advantages over a nerve cuff. First, by interfacing with a subset of neurons within a fascicle, it has the potential to be more selective. Second, while a nerve cuff may require over 250 μA to evoke muscle contractions from target muscles, intrafascicular electrodes achieve the same results with less than 50 μA and display more graded recruitment curves [24]. Third, by implanting multiple microelectrodes within a fascicle, where fibers in the same fascicle target the same muscle group, interleaved stimulation can be used to improve

fatigue resistance in an FES system [25]. However, long-term implantation of these electrodes has not been fully tested.

ISMS has been demonstrated to generate graded forces as a function of stimulus amplitude, though nerve cuff stimulation is able to produce greater maximum muscle forces [26]. Typical ISMS current amplitudes range between 10 – 240 μA [27]. In addition, it remains a challenge to generate selective, reproducible movements with ISMS [20]. This lack of selectivity is, in part, due to the difficulty in targeting the motor pools of the ventral spinal cord [28]. Finally, it is interesting to note that, with ISMS in the ventral laminae of the spinal cord, sensory neurons are typically activated at lower stimulus amplitudes than motoneurons, resulting in post-synaptic activation of the motoneurons [29, 30]. These ventral laminae contain fibers, many of them afferents, synapsing onto efferent cell bodies and it is the fibers, not the cell bodies, which are the sites of membrane depolarization [29, 31]. Indeed focal ISMS has been shown to result in extensive spread of activity, causing antidromic activation of afferents across multiple spinal levels both rostral and caudal to the stimulus site [29, 30].

Table 1.1 Qualitative comparison of existing FES interfaces by performance metrics.

Interface	Selectivity	Threshold	Force Recruitment Rate	Force Recruitment Magnitude
Surface	muscle	very high	very steep	large
Epimysial/Intramuscular	muscle	high	steep	large
Extraneural	fascicle	moderate	steep	large
IFMS	sub-fascicle	low	graded	moderate
ISMS	muscle	low	graded	moderate

Given the benefits and drawbacks of the different interfaces, intraneural stimulation appears to have potential for applications in FES systems because of its selectivity and low power consumption, but has not been explored to the extent that other interfaces have. However, it is worth testing the use of this interface with neural structures other than the peripheral nerve

in an effort to improve on some of the limitations of IFMS. While penetrating high-density arrays can provide many channels for selective activation of multiple peripheral targets, multiple interfaces would be required to access the nerves of the extremities. In addition, distal portions of nerves, where the fascicular organization is greatest, are difficult to access. Finally, peripheral nerves in general are mobile and poorly protected, which results in a mechanically unstable interface. Ventral root (VR) stimulation is therefore a logical choice because it provides a mechanically stable location with a high density of motor fibers that can be activated directly. Dorsal root ganglion (DRG) stimulation, on the other hand, may achieve the same benefits as ISMS, such as recruiting slow motor fibers at a threshold lower than fast motor fibers, while also providing a mechanically stable interface location. It is worth exploring both VR and DRG stimulation to evaluate the extent to which we observe these benefits.

1.4 INTERFACING WITH THE SPINAL ROOTS

VR microstimulation with penetrating microelectrodes directly activates motor fibers. In anaesthetized cats, O'Donovan and colleagues stimulated individual neurons in the VR and characterized the physiological properties of responding motor units [32]. They measured conduction velocity, electromyograms (EMG) and the contractile force of the quadriceps. Though the relationship between stimulus current and patellar force output was not reported, they did use the force traces to determine the fatigue resistance of the muscle. Their results suggested that body-weight supporting forces could be generated in cats. The current threshold at which electromyogram responses could be detected was found to range between 5 and 10 μA. Of greatest interest were their observations on the relationship between stimulus intensity and EMG

response: As the stimulus intensity increased, the evoked EMG response increased incrementally. Moreover, the earliest EMG response was confined to a single muscle and the response stayed confined to that muscle over a "substantial" increase in stimulus amplitude [32].

These findings for VR microstimulation suggest that an electrical interface with the VR is feasible, but unexplored in the context of FES. Little work has been done exploring VR microstimulation, especially to examine the functional responses in muscle activity. In addition to the potential benefit of having a mechanically stable interface as with a DRG interface, VR microstimulation provides a central site for accessing all of the motor fibers innervating target muscles.

Primary afferent stimulation offers an alternative approach, by which motor fibers are recruited through trans-synaptic activation. In previous electrophysiology experiments in our lab, we stimulated afferents in the DRG while recording in the sensory cortex of cats [33]. We noted motor responses in the hindlimb at low current amplitudes and thus considered using DRG microstimulation to restore motor function. The DRG offer an interesting option for an implant location. Stimulation within the DRG would likely activate spinal circuitry in similar fashion to ISMS, which tends to activate sensory neurons before motoneurons [30]. The motor responses evoked by DRG microstimulation would be the result of post-synaptic activation of motor fibers in the spinal cord and therefore might be similar to evoked motor responses from ISMS. Indeed, DRG microstimulation may demonstrate recruitment of movement primitives as in ISMS without the difficulty of electrode placement and with the low power consumption of IFMS. In addition, as with a VR interface, a DRG electrode interface would be more mechanically stable than other nerve interfaces because the spinal roots move little during limb movements.

1.5 SPECIFIC AIMS

This work evaluates the performance of a novel interface for restoring motor function in paralyzed patients with intact peripheral motor fibers using functional electrical stimulation (FES). We identified two possible neural structures for electrode implantation: the VR and the DRG, which contain, respectively, only motor fibers or only sensory neurons. Both locations are mechanically stable and would require little current to effect a response in comparison to other interfaces. The spinal roots provide access to the varied targets of the limb. We hypothesize that VR stimulation will provide the same benefits as IFMS whereas DRG stimulation will provide the same benefits as ISMS. Therefore, these two interfaces were evaluated separately and then compared along a set of performance criteria. To this end, we have two specific aims, which use two different approaches, to engage this problem.

1.5.1 Specific Aim 1

Characterize the functional responses of the hindlimb to ventral root or dorsal root ganglion microstimulation with varying stimulus parameters. Little work has been done to document muscle recruitment in response to VR or DRG microstimulation. Several metrics will be used to compare the effectiveness of microstimulation in the two different nervous tissues, including the slope of the force recruitment curve, the current amplitude to recruit one muscle group before recruiting its co-contractor muscle group, the distribution of thresholds to observe muscle recruitment, and the ability to access the varied muscle groups of the hindlimb. These metrics gauge our ability to evoke controlled, graded recruitment of targeted muscle groups with little current. In rats and cats, single channel microstimulation in lower lumbar DRG or VR will be

tested at varying amplitudes and frequencies while electromyograms (EMG) will be used to determine which muscle groups responded. A force transducer will also be used to measure the three-dimensional isometric endpoint force of the hindlimb. The resulting metrics will be compared between the DRG and VR microstimulation approaches tested here and with published results for other electrode interfaces to deduce the potential of the DRG and VR as effective interface locations. We hypothesize that single channel microstimulation in DRG will yield functional responses similar to those observed from ISMS, with broad force recruitment curves, low current thresholds, and discrete, categorical force vectors that result from activating reflex pathways. VR stimulation should have even lower thresholds, comparable to IFMS of peripheral nerve, with broad recruitment curves and good selectivity.

1.5.2 Specific Aim 2

Characterize the pattern of fiber recruitment in a computational model of ventral root or dorsal root ganglion microstimulation. Knowing the numbers and sizes of fibers that are activated in response to microstimulation would help determine the mechanisms by which we observe the functional responses addressed in Specific Aim 1. Electrophysiological methods alone are not sufficient to provide information on these mechanisms. To this end, we shall develop a computational model that predicts the recruitment of axons as a function of stimulus and environmental factors. While several models exist for predicting recruitment of neuronal fibers in response to extraneural stimulation, the pattern of neuronal recruitment around an intraneural electrode as a function of stimulus intensity is poorly understood. Using this computational model, we shall vary stimulus intensity and tissue parameters, and estimate the number and types of neurons activated in a volume of tissue. This model will be used to test the hypothesis that

recruitment of fibers in response to microstimulation is not biased toward larger fibers over smaller fibers. This information will help in understanding the mechanisms behind the functional responses evoked in electrophysiology experiments as well as help determine design criteria for an FES system using this interface scheme.

2.0 MOTOR RECRUITMENT IN RESPONSE TO VENTRAL ROOT OR DORSAL ROOT GANGLION MICROSTIMULATION IN RATS

Here we present the results of electrophysiology experiments in rat to address Specific Aim 1. Single channel microstimulation in the VR or DRG selectively recruited hindlimb muscles, activity that we detected via electromyograms and a force transducer. Analysis of these data provided information for comparing the quality of these interfaces to each other and to other interfaces, such as IFMS and ISMS.

2.1 INTRODUCTION

In designing interfaces for stimulating nervous tissue to evoke motor responses, researchers consider several design criteria, including power consumption, selectivity, fatigue resistance, and the ability to produce graded, forceful limb movements [5, 15]. To examine VR and DRG interfaces, we began by characterizing the functional responses of the hindlimb to VR or DRG microstimulation with varying stimulus parameters. We deemed a response functional if it could make a nontrivial contribution to a significant limb movement, such as producing sufficient force to allow the subject to stand or walk. Given these responses, we measured: (1) the threshold to observe activation, (2) the current amplitude range to recruit one muscle group before recruiting its mutual antagonist group, (3) the slope of the force recruitment curve, and (4) the magnitudes

of the force vectors achieved. We used these metrics to assess these interfaces' abilities to meet some of the design criteria.

The threshold at which muscle activity could first be observed in an electromyogram, along with the slope of the force recruitment curve, corresponds to the amount of power that the interface will require. O'Donovan and colleagues measured the threshold at which electromyograms were detected in response to VR stimulation at 5 – 10 μA [32]. ISMS, on the other hand, has higher thresholds of 10 – 240 μA, observed with EMG, palpation or visual inspection [27]. The slope of the force recruitment curve also provides an estimate of the interface's ability to evoke controlled, graded forces, which is critical for practical function of an FES system. Using a force transducer attached to the patellar tendon, Bamford and colleagues plotted normalized peak twitch force against stimulus amplitude and demonstrated that ISMS provides more graded force recruitment than nerve cuff stimulation [26]. Similarly, Normann and colleagues measured the recruitment of peak twitch gastrocnemius force to be approximately 1 N/μA in response to IFMS in the sciatic nerve [34].

The selectivity of the interface is also critical for developing a useful interface. Different approaches have been used in describing the selectivity of an interface. Durand and colleagues explored fascicular selectivity in response to nerve cuff stimulation of the hypoglossal nerve [35]. They defined a selectivity index as the ratio between the recorded voltage of the target fascicle or muscle and the sum of the voltages of all recorded fascicles or muscles. This approach was facilitated by their ability to access all neurons innervating the muscles supplied by the hypoglossal nerve. McDonnall and colleagues used a qualitative approach, observing single muscle twitches in response to IFMS in the sciatic nerve before increased current resulted in twitching of other muscles [36]. In the following experiments, the range of current amplitudes

over which one target muscle is recruited before its mutual antagonist muscle group is also recruited assessed this selectivity criterion. An interface would not be useful if it tended to activate both a muscle and its mutual antagonist simultaneously.

Finally, the force vectors achieved through single-channel neural stimulation should be of sufficient magnitude to combine them and produce useful movements, such as standing or walking. Many investigators measure muscle contraction forces in response to stimulation [26, 34]. Lemay and Grill, however, measured fixed endpoint forces in response to ISMS at approximately 1N [16]. This endpoint measurement can offer a simple assessment of the interface's ability to generate forces sufficient to move a significant percentage of body weight.

Having outlined criteria for judging the performance of a functional electrical stimulation (FES) interface, we began examining VR and DRG interfaces. Because VR microstimulation activates motor fibers directly, we expected this interface to perform in similar fashion to IFMS of the peripheral nerves. There are few differences between VR and IFMS interfaces, the most important of which are the decreased density of motor fibers in the peripheral nerves and the altered distribution of those motor fibers by target of innervation. On the other hand, due to a very different, indirect mechanism of evoking motor responses, we expected DRG microstimulation to perform in similar fashion to ISMS. Gaunt and colleagues [30] observed that ISMS activated sensory afferents at lower current amplitudes than motor efferents. They concluded that sensory afferents activated through ISMS excited motor fibers trans-synaptically, resulting in electromyogram responses. Similarly, with the DRG comprising only sensory afferents, microstimulation will also activate primary afferent neurons, which may in turn excite motor fibers trans-synaptically. The performance of ISMS includes motor responses due to direct

activation of motor fibers as well as the trans-synaptic activation just described, which may affect our comparison between ISMS and DRG microstimulation.

To assess VR and DRG interfaces, we implanted electrodes into rat VR and DRG, as well as cat DRG, for single-channel stimulation. We measured fixed hindlimb endpoint forces with a three-dimensional force transducer and, additionally, measured EMG in hindlimb muscles simultaneously. Analysis of the force and EMG responses to stimulation provided the metrics for comparison described above. While VR stimulation demonstrated significantly decreased thresholds for muscle activation and broader force recruitment, DRG stimulation evoked significantly larger forces. We conclude that neither interface is inherently superior to the other and both warrant further investigation.

2.2 METHODS

This experiment was designed to record functional responses (i.e. electromyograms and endpoint forces) evoked by microstimulation in the VR or DRG. The surgical procedures provided access to the spinal roots for stimulation as well as the hindlimb and its muscles for measuring the functional responses. Stimulus frequency, amplitude, and electrode location were varied in order to explore the effects of these parameters.

2.2.1 Surgical preparation

All procedures were approved by the Institutional Animal Care and Use Committee (IACUC) of the University of Pittsburgh. Experiments were conducted in healthy adult rats (300 - 500 g).

Throughout the experiment, the subject's body temperature was maintained at 37 °C using an electric heating pad and a rectal thermometer. Under isoflurane anesthesia (1.5 - 2.5%), we performed a laminectomy to expose the spinal cord and spinal roots at the 5^{th} and 6^{th} lumbar segments (L5 and L6). Following the laminectomy, we transferred the animal to a spinal frame with the torso supported and the hindlimbs allowed to move freely. The head was fixed in a stereotaxic frame and vertebrae clamps and hip pins were used to stabilize the spine. When stimulating in the VR, we additionally performed a dorsal rhizotomy to expose these roots. This rhizotomy helped visualize the VR for improving placement of the stimulating electrode in the VR and assured that responses to stimulation were not due to activation of spinal reflexes via the dorsal roots. At the end of the experiment, the animal was euthanized with a 5 mg/kg dose of potassium chloride.

2.2.2 Stimulation and data acquisition

Using a micromanipulator, we implanted a single wire electrode (MicroProbes, Gaithersburg, MD) for electrical microstimulation into the exposed DRG. These parylene-insulated electrode wires were made of a platinum-iridium alloy with a diameter of 75 μm and an impedance of approximately 0.1 MΩ at 1 kHz. A stainless steel wire placed in the epidural space along the spinal cord acted as the return electrode. Stimulus waveforms were generated and delivered using an RX7 microstimulation system (Tucker-Davis Technologies, Alachua, FL). These waveforms were biphasic and charge-balanced, with a cathodic-leading 200 μs pulse followed by a 400 μs anodic pulse. Stimuli were delivered in 500 ms trains at frequencies of 10 – 1000 Hz and at amplitudes of 1-100 μA (cathodic phase). We randomized stimulus parameters that varied

within a trial, including frequency and amplitude, with five repetitions for each stimulus condition.

After performing these stimulus trials, we removed the stimulating electrode and re-inserted it into a different location in the DRG, then repeated the stimulation trials. Removal and re-insertion of the stimulating electrode wire was repeated up to six times per DRG. Then we performed dorsal rhizotomies, cutting the proximal dorsal roots and exposing the VRs. In similar fashion, we implanted each VR with a single wire electrode, removing and re-inserting it up to six times, and performing all stimulus trials per insertion of the stimulating electrode wire. All stimulation in these rats was single-channel and each rat provided both the VR and DRG stimulation data.

We then implanted pairs of percutaneous stainless steel electrodes using hypodermic needles into the muscles of the hindlimb, ipsilateral to the implanted spinal roots. These muscle groups included the tibialis anterior (TA), medial gastrocnemius (MG), biceps femoris (BF), semitendinosus (ST), vastus lateralis (VL), and vastus medialis (VM) muscles. For each of the implanted hindlimb muscles, we recorded a bipolar electromyogram (EMG) at 4.9 kHz in response to microstimulation on an RZ2 multichannel workstation (Tucker-Davis Technologies, Alachua, FL). A stainless steel wire under the skin acted as ground. Finally, the animal's foot was mounted to an insulated aluminum rod that was attached to a rigidly fixed six-axis force transducer (ATI, Apex, NC). This force transducer recorded the endpoint force of the ipsilateral hindlimb in response to microstimulation. Force data were recorded at 1 kHz using a custom-built LabVIEW program (National Instruments, Austin, TX). A transformation matrix was applied to these data to correct for three-dimensional angle and displacement differences

between the location of the animal's foot at the end of the rod and the location of the force transducer (Figure 2.1).

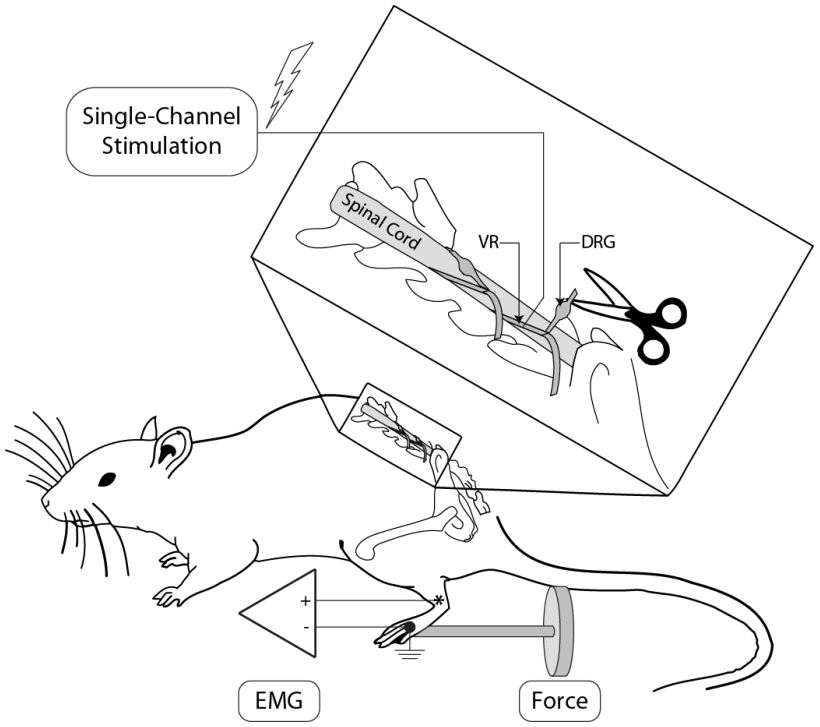

Figure 2.1 Schematic representation of experimental setup. A laminectomy provides access to the spinal roots. In response to single-channel electrical stimulation, a force transducer measures fixed endpoint forces and wires implanted in the muscles measure EMG. For VR stimulation, a dorsal rhizotomy cuts the dorsal root, exposing the VR and leaving it intact.

2.2.3 Data analysis

Using a 4th order Butterworth filter, EMG data were notch filtered to remove 60 Hz line noise and then lowpass filtered, with a cutoff frequency of 500 Hz. These data were rectified, aligned with the beginning of each stimulus pulse train, and then averaged across the five repetitions for each stimulus condition. These averaged data were used to identify responses in the EMG to electrical stimulation. We used this EMG signal as a sensitive measure to identify which muscle groups were activated in response to stimuli as well as the threshold at which a response could be

detected. We defined threshold as the current amplitude at which the EMG signal showed a response to microstimulation. The EMG signal indicated a response if the mean of the EMG response signal was greater than the mean plus two standard deviations of the EMG signal without stimulation. Above this cutoff level, there is only a 5% chance that signals are indistinguishable from background noise. An additional criterion for threshold was that all subsequent responses at higher stimulus amplitudes were also above this cutoff.

Force data were processed in similar fashion to EMG data. First, a 4^{th} order Butterworth lowpass filter smoothed the data with a cutoff frequency of 20 Hz. These data were then aligned to the beginning of each stimulus pulse train and averaged. As in the case of EMG data analysis, we used mean plus two standard deviations of baseline force to find threshold. We then estimated the slope of the recruitment curve using linear regression from the threshold to the amplitude at which 75% of maximum recruitment was achieved. Finally, we calculated the magnitude and direction of the averaged force responses.

2.3 RESULTS

The primary aim of these electrophysiology experiments was to characterize the functional responses in the hindlimb to microstimulation in the lumbar VR or DRG and then compare the potential quality of an interface implanted in these tissues. The frequency, amplitude and electrode location were varied to examine their effects on recruitment of specific muscle groups and endpoint forces. We describe the effects of varied parameters on EMG responses. We then present data on power consumption and selectivity. Next, we focus on force recruitment,

examining both recruitment rate and magnitude. Finally, we address the possibility that DRG stimulation resulted in current spread to the VR, directly activating motor neurons.

2.3.1 Response waveform patterns

Overall, we performed single-channel stimulation on a total of 81 channels across five rats and four tissue locations (see Table 2.1). We began by examining the EMG signals for their dependence on stimulus amplitude and frequency. Figure 2.2 shows medial gastrocnemius EMG traces in response to varying stimulus parameters for VR stimulation on channel 14 of rat 2 and DRG stimulation on channel 1 of rat 2. As expected, increased current amplitude resulted in increased magnitude of the EMG signals. Altering the stimulus frequency resulted in EMG signals that oscillated at the stimulus frequency. With both ventral and dorsal spinal roots cut, microstimulation did not result in EMG responses, nor were there oscillations following the stimulus frequency. This result suggested that stimulation was isolated to the spinal roots and current did not spread into other structures at the amplitudes tested. In addition, there was a significant difference in these responses as a function of stimulus frequency. As the frequency was increased from 50 to 100 Hz, the amplitude of the EMG signals remained consistent. However, as the frequency was further increased to 300 Hz, the EMG amplitude dropped significantly, as if the system were unable to follow this higher rate of activity. Further examination of the temporal pattern of these signals provided insights into this frequency-dependent behavior.

Table 2.1 Number of stimulus channels across rats and stimulation sites. Five rats and four stimulation sites were tested. All stimulation was single-channel and these five rats provided both the VR and DRG stimulation data. Damage to DRG L5 in Rat 4 prevented stimulation in that tissue.

	Rat 1	Rat 2	Rat 3	Rat 4	Rat 5
VR L5	4	4	6	6	6
VR L6	3	4	4	5	5
DRG L5	3	4	4	0	4
DRG L6	4	4	3	4	4

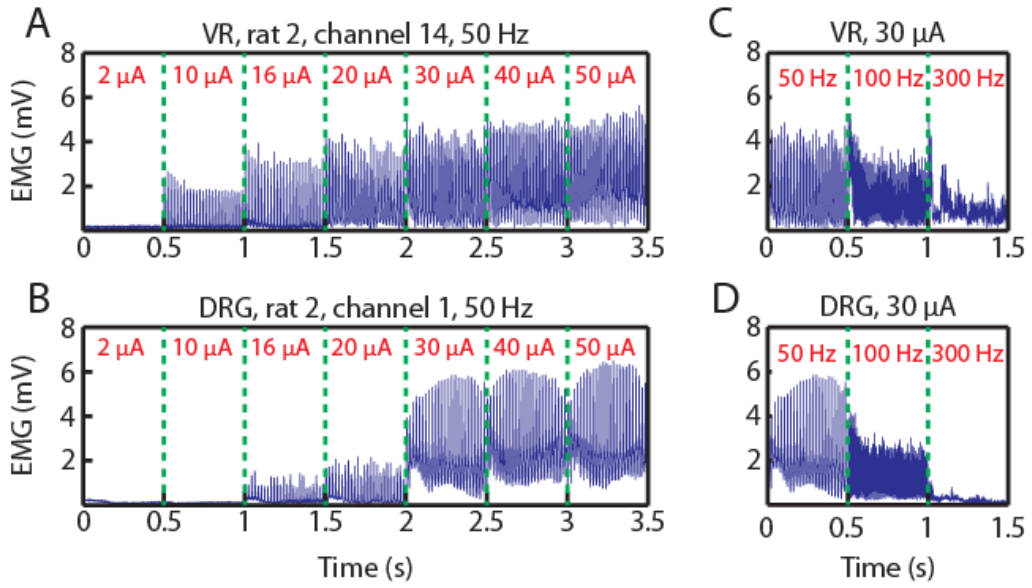

Figure 2.2 MG EMG response depends on stimulus amplitude and frequency. These traces are typical EMG signals for medial gastrocnemius recorded in response to VR (top) or DRG (bottom) microstimulation. (A, B) EMG response increases as stimulus amplitude increases, with stimulus frequency at 50 Hz. (C, D) However, as the frequency increases beyond 300 Hz, the steady-state EMG response is diminished, with stimulus amplitude at 30 µA. These data are taken from stimulation in rat 2, channels 14 (VR) and 1 (DRG).

Over the duration of the stimulus, the EMG signals exhibited a characteristic pattern of activity. Following stimulus onset, there was an initial transitional phase in the first 200 ms, followed by a steady state response lasting until the end of the stimulus pulse train at 500 ms. The steady state response is thus measured as the mean of the last 300 ms of the processed EMG signal. The steady state component represents sustained activation of a muscle. Therefore, we

performed subsequent analyses for these steady state responses. Figure 2.3 illustrates the range of MG steady state responses for stimulus currents at twice threshold across all stimulus channels and rats. Using an analysis of variance, the responses to 300 Hz stimulation were found to be significantly smaller than for 50 or 100 Hz stimulation, for both VR and DRG stimulation ($p < 0.01$). This result was consistent for each of the muscles from which we recorded.

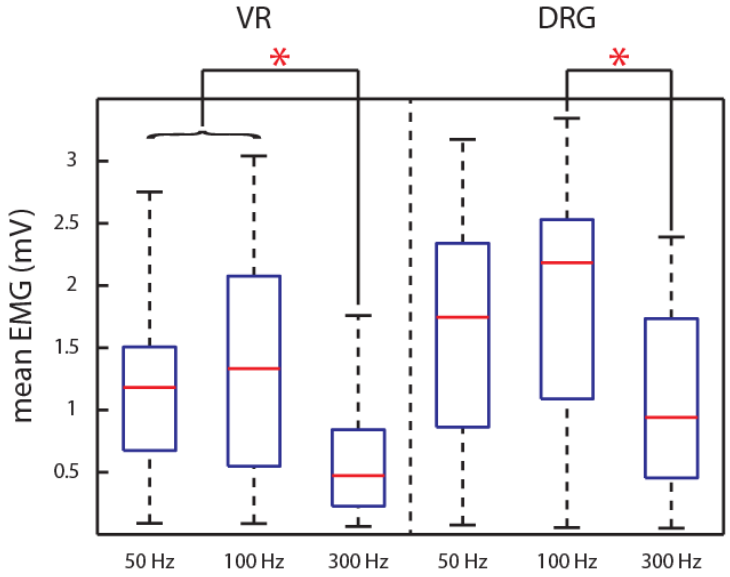

Figure 2.3 Steady-state MG EMG responses as a function of frequency and tissue location. An analysis of variance on the distributions of EMG response magnitudes demonstrates a significant decrease in EMG magnitudes at 300 Hz for both VR and DRG stimulation. Boxplots illustrate the 5th, 25th, 50th, 75th and 95th quantiles. Stimulus channels are grouped across rats, including 47 VR channels and 34 DRG channels. Asterisks denote a significant difference between distributions ($p < 0.01$).

2.3.2 EMG threshold and muscle selectivity

The distribution of threshold amplitudes for VR and DRG stimulation is quite different across stimulus channels and rats (Figure 2.4). Having recorded EMG from six hindlimb muscles simultaneously, the threshold represents the lowest stimulus amplitude that resulted in an EMG response from any of the six muscles. Using the non-parametric Mann-Whitney U-test for

equivalence, we found the distribution of threshold amplitudes in response to VR microstimulation, with a median of approximately 12 μA, to be significantly smaller and narrower than threshold distributions in response to DRG microstimulation, with a median of approximately 25 μA ($p < 0.01$, n = 47 VR channels and 34 DRG channels). Stimulus frequency did not play a significant role in these threshold distributions.

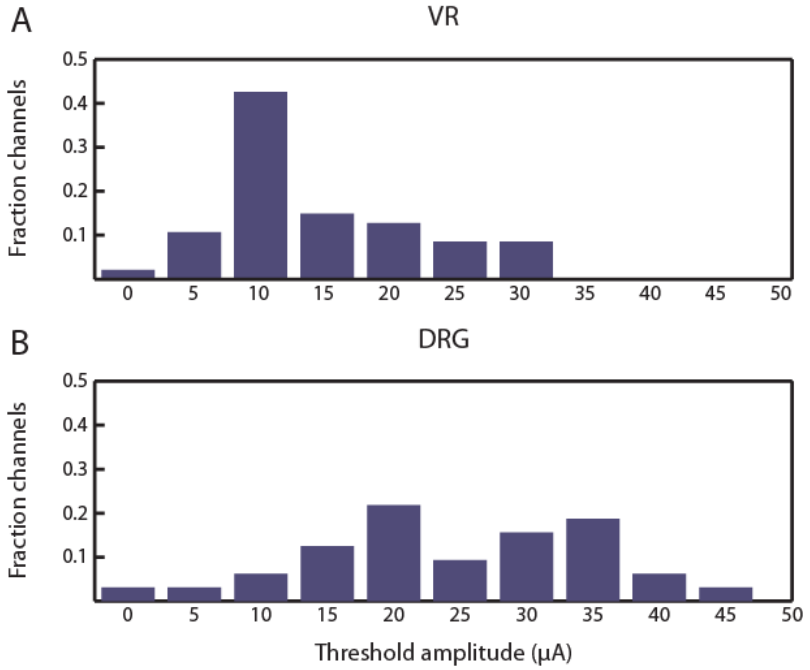

Figure 2.4 Distribution of thresholds to observe any EMG response to VR or DRG stimulation. These two distributions are significantly different (Mann-Whitney U-test, $p < 0.01$), with medians of 12 μA and 25 μA for VR and DRG stimulation, respectively. VR stimulation (A) demonstrates a gamma distribution of thresholds to recruit an EMG signal and DRG stimulation (B) a broader distribution. Data includes 47 VR channels and 34 DRG channels with stimulation at 50 Hz.

Next, we observed which muscles were activated at threshold. Figure 2.5 illustrates the distributions of ankle-actuating muscles activated at threshold, given location of stimulus electrode. Stimulation in the 5th lumbar DRG resulted in approximately equal observations of recruiting TA or MG muscles at threshold. Stimulation in the 6th lumbar DRG, however, showed a strong bias favoring recruitment of MG over TA. Both L5 and L6 VR stimulation resulted in approximately equal likelihoods of recruiting either TA or MG at threshold. Given that VR

stimulation results in direct activation of motor efferents, we might assume that these distributions of muscles recruited are a direct result of the relative quantities of efferents supplying the TA and MG in these VR.

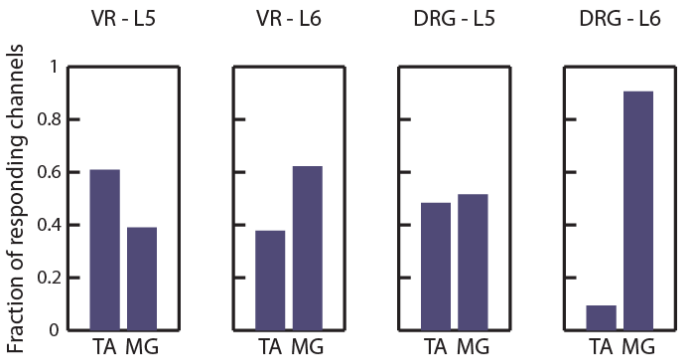

Figure 2.5 Distribution of ankle-actuating muscles recruited at threshold depends on stimulus electrode location. DRG-L6 stimulation predominantly recruits MG, whereas the other stimulus locations demonstrated approximately equal likelihood for recruiting one of these antagonist muscles at threshold. These distributions are presented as fractions of the total number of channels that did *not* show activation of antagonist muscles at threshold. A total of 26, 21, 15, and 19 stimulus channels were tested for VR L5, VR L6, DRG L5, and DRG L6, respectively.

To further understand our ability to selectively recruit muscle groups, Figure 2.6 illustrates the inverse cumulative distributions of the difference in threshold amplitudes to recruit mutual antagonist muscle groups. The difference in threshold (ΔI_{th}) is measured as the difference between the threshold to activate a muscle and the threshold to activate its mutual antagonist muscle (e.g. TA and MG for ankle flexion/extension). For all stimulus channels, this difference in threshold is greater than or equal to zero, by definition of the inverse cumulative distribution. There is then a significant decrease in the fraction of stimulus channels that demonstrated at least 2 μA between these two thresholds. The patterns in these cumulative distributions are similar between VR and DRG microstimulation. We found no significant difference between these distributions using a Mann-Whitney U-test ($p = 0.9$). DRG stimulation did not offer improved selectivity over VR stimulation in spite of having a large bias toward recruiting MG over TA, as

illustrated in Figure 2.5. Typically, the difference between the threshold to activate the first muscle and that to activate the second muscle, if there is a difference, is between 2 – 20 μA. These differences in threshold are not trivial, given the thresholds for evoking EMG signals in both VR and DRG microstimulation (Figure 2.4). Differences of 2 – 20 μA represent approximately 15 – 150% and 10 – 80% of the thresholds to recruit EMG in response to VR and DRG stimulation, respectively.

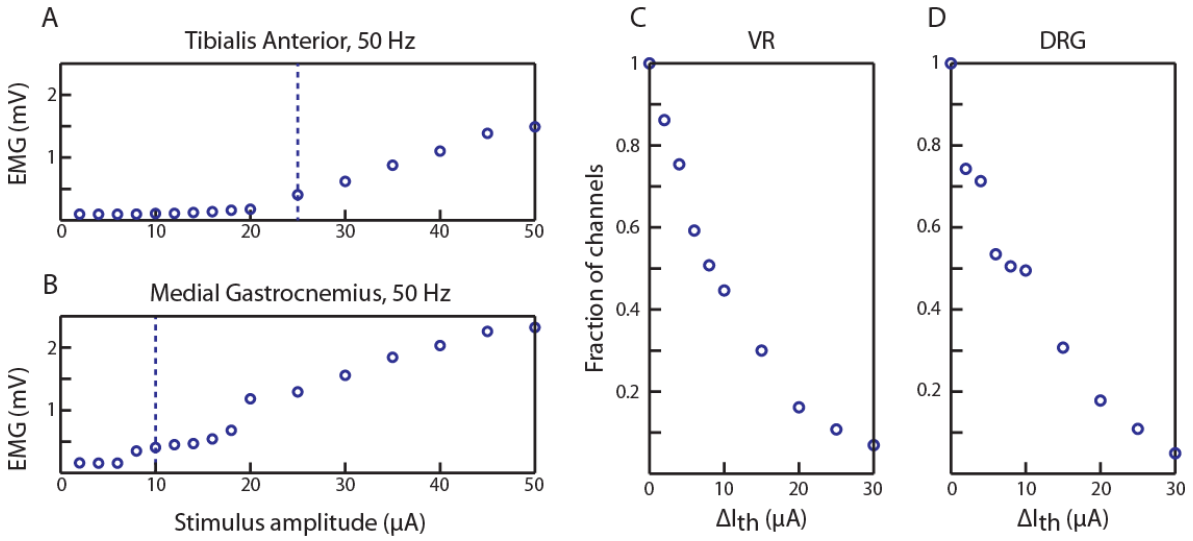

Figure 2.6 Selectivity for target muscle. (A, B) EMG recruitment curves for TA and MG muscles in response to VR stimulation on rat 2, channel 14 (same channel as for figure 2.2). A vertical line denotes the threshold at which activity was detected. (C, D) Inverse cumulative distribution of the difference in thresholds (ΔI_{th}) of mutual antagonist muscle groups for VR and DRG stimulation. VR stimulation demonstrates improved selectivity in that a greater fraction of stimulus channels showed larger differences in thresholds for recruiting within a mutual antagonist muscle group. Data for (C and D) are taken across the 47 and 34 VR and DRG stimulus channels at 50 Hz, respectively, and compare muscle groups that flex and extend the ankle or knee joints.

2.3.3 Force recruitment rate and magnitude

We explored endpoint force recruitment in response to VR or DRG stimulation. Figure 2.7 (A, B) shows the magnitude of the endpoint forces as a function of time in response to

several stimulus amplitudes. These traces are for a single stimulus channel in the VR or DRG in rat 1. By varying the stimulus amplitude, we can then describe the recruitment curve. Figure 2.7 (C, D) depicts the approximately linear relationship between stimulus amplitude and force magnitude. The patterns of force recruitment were not significantly different between VR and DRG stimulation. Of particular interest is the slope of the recruitment curve as it represents our ability to produce controlled, graded responses to stimuli.

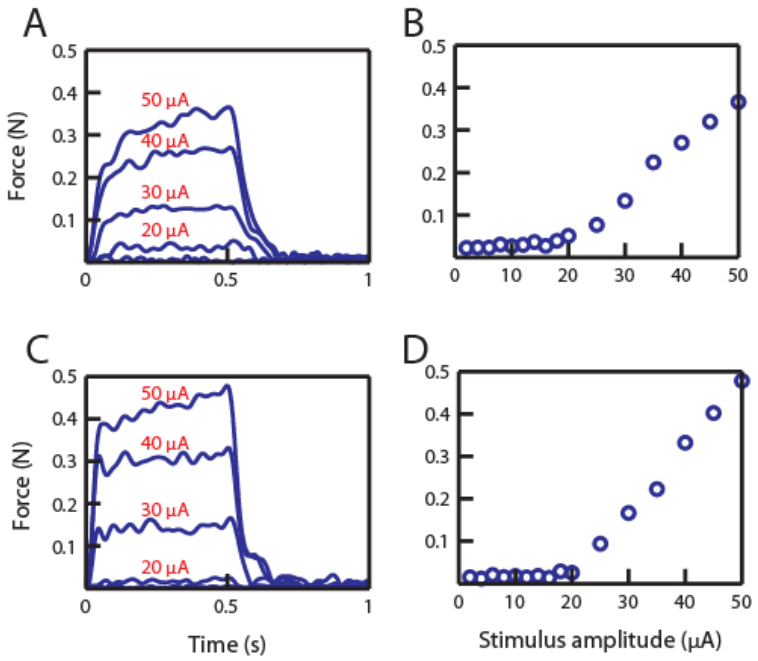

Figure 2.7 Force magnitude as a function of time and stimulus amplitude. (A) Endpoint force magnitude over time in response to 50 Hz VR stimulation on rat 1, channel 28 at amplitudes of 20, 30, 40, and 50 µA. The stimulus duration was 500 ms. (B) Force recruitment curve plotted against stimulus amplitude for this same stimulus channel. (C, D) Force recruitment in response to 50 Hz DRG stimulation on rat 1, channel 39. The slopes were measured from these recruitment curves at current amplitudes above threshold.

Figure 2.8 shows the distributions of the slopes of the recruitment curves in response to VR or DRG microstimulation across stimulus channels. We performed a Mann-Whitney U-test, which showed that the distributions of slopes for these two tissues were *not* significantly

different ($p = 0.17$, $n = 31$ responding VR channels and $n = 28$ responding DRG channels), with medians of 0.015 and 0.017 N/μA for VR and DRG stimulation, respectively. There was little difference in the slopes at stimulus frequencies of 50 or 100 Hz. However, the slopes showed a significant decrease at 300 Hz for both tissues using the Mann-Whitney U-test ($p < 0.01$ for $n = 30$ VR channels, $p = 0.04$ for $n = 28$ DRG channels), with medians of 0.006 and 0.01 N/μA for VR and DRG stimulation, respectively. This result would suggest that both VR and DRG stimulation could achieve similarly controlled, graded force recruitment.

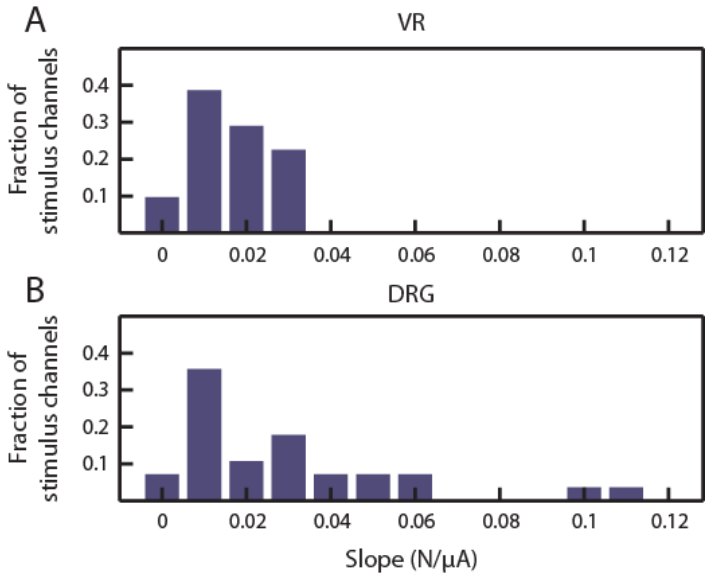

Figure 2.8 VR and DRG stimulation result in graded force recruitment. (A) The distribution of force recruitment curve slopes in response to VR stimulation was narrow and small. (B) The distribution of slopes in response to DRG stimulation was similar to that of VR stimulation. These small slopes suggest some control over force recruitment. Distributions include all 31 responding VR channels and 28 responding DRG channels at 50 Hz stimulation.

In addition to the muscles recruited at threshold as illustrated in Figure 2.5, most stimulus channels were able to recruit all of the muscles from which we recorded, at sufficiently high stimulus amplitudes. Indeed, each of the seven different muscles from which we recorded EMG were represented by at least one VR or DRG stimulus channel, in both L5 and L6, demonstrating these interfaces' capacities for accessing these muscles. Of greater interest, though, is the ability

to generate useful muscle activation patterns. That is, can VR or DRG microstimulation result in activation of a set of muscle groups resulting in limb states or movement primitives that we could combine to form, for example, a standing or walking pattern? Figure 2.9 illustrates the distributions of the four different combinations of muscle activation patterns, represented by combining ankle flexion or extension with knee flexion/extension. These patterns of muscle activation represent the combinations of muscles that produced EMG activity at threshold. TA and MG activation result in ankle flexion and extension, respectively. Knee flexion results from BF or ST activation, while knee extension results from VL or VM activation.

The first bar in these distributions represents activation of antagonist groups, such as TA and MG, which means that, at threshold, stimulation simultaneously activated motor neurons innervating antagonist groups. The second bar represents activation of a single muscle group at threshold. For muscle combinations, VR stimulation resulted in slightly increased likelihoods of achieving knee flexion in concert with ankle extension. All four combinations were represented, but simultaneous activation of ankle flexors with knee extensors was rarely observed.

Ankle extension with knee flexion is a useful combination for achieving forward propulsion during locomotion and is defined as the end of stance phase by Goslow and colleagues [37]. DRG stimulation demonstrated a strong bias toward generating forward propulsion through this combination of ankle extension with knee flexion, but the overall pattern of muscles activated was similar to that of VR stimulation. It is important to remember, however, that these distributions are based on single channel stimulation and detection of muscle activity at threshold levels, not the level of muscle activity at higher intensities. In the next section we shall examine force output as the stimulus intensity is increased.

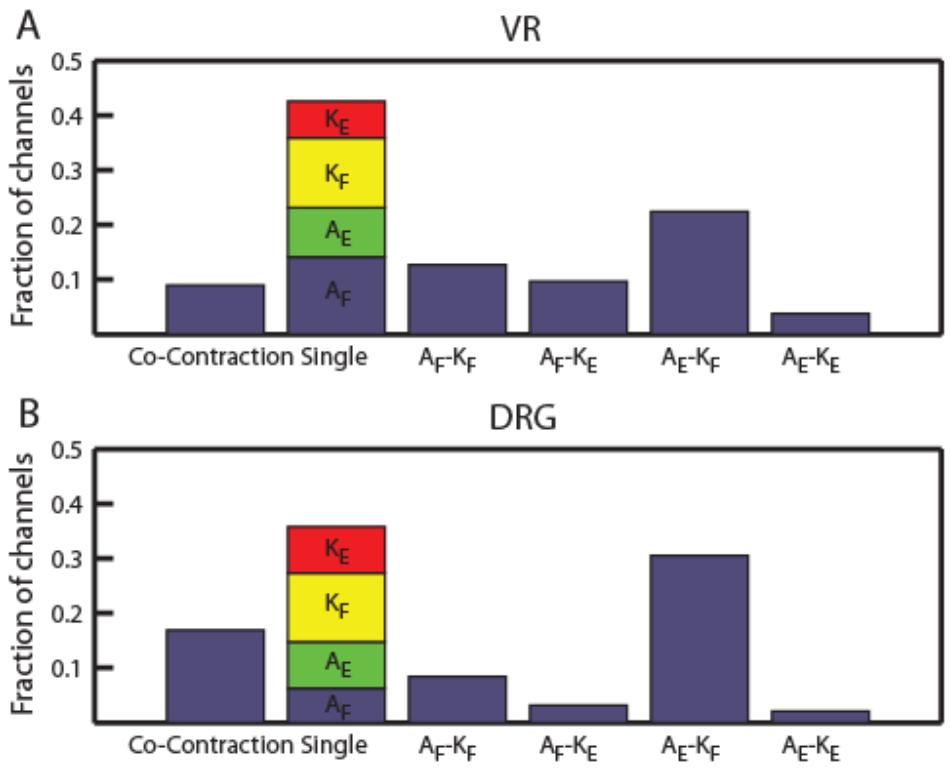

Figure 2.9 Patterns of muscles recruited at threshold. (A) VR stimulation in L5 and L6 rarely produced ankle extension with knee extension, but often produced ankle extension with knee flexion. A single muscle was usually recruited at threshold and ankle and knee flexors and extensors were all represented. (B) DRG stimulation in L5 and L6 produced a similar distribution of muscle recruitment patterns compared to VR stimulation, but with a greater likelihood of producing ankle extension with knee flexion. A and K refer to ankle and knee, respectively; F and E subscripts refer to flexion and extension, respectively. Data are taken across the 47 and 34 VR and DRG stimulus channels, respectively.

Figure 2.10 illustrates the vectors of the hindlimb endpoint forces in the sagittal plane in response to stimulation. For each of the VR and DRG stimulus channels, we plotted force data for amplitudes at twice the threshold for eliciting an EMG response. DRG stimulation produced larger forces than VR stimulation. Interestingly, the directions of these forces were quite similar for VR and DRG stimulation. An adult rat weighing approximately 400 g would require a hindlimb extension of approximately 1 N to support a quarter of its bodyweight for standing. This force level is illustrated on the plots as with a horizontal red line. With only a single

stimulus electrode, DRG stimulation demonstrated the capacity to achieve forces sufficient for standing, and VR stimulation nearly so.

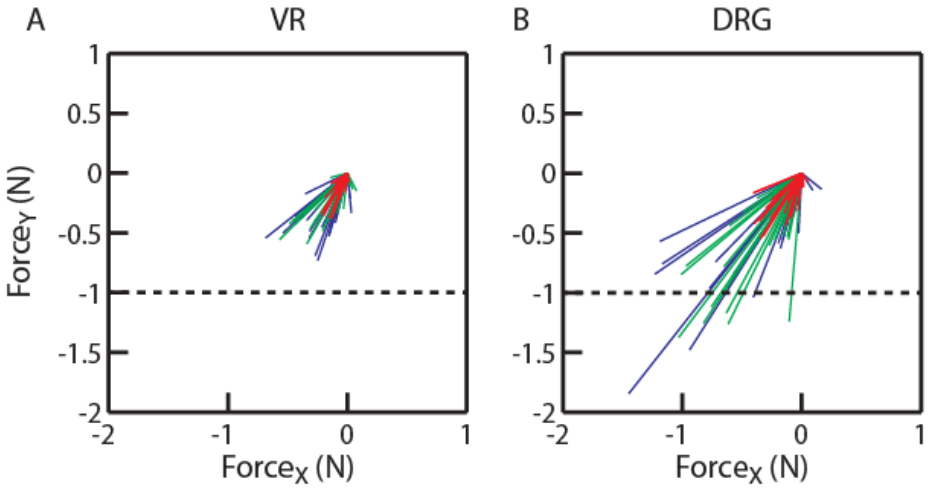

Figure 2.10 Endpoint force vectors in the sagittal plane at twice threshold. (A) Single-channel VR stimulation produced caudal extension of the hindlimb at almost 1 N. (B) DRG stimulation tended to produce much greater forces, but the directions were the same as with VR stimulation. Dashed horizontal lines at -1 N denote vertical force required for the hindlimb to lift 25% body weight of a 400 g rat. Force vectors for stimulus frequencies of 50 Hz (blue), 100 Hz (green) and 300 Hz (red) at amplitudes of twice threshold are reported for all VR and DRG stimulus channels.

2.3.4 Verifying current spread in tissue

We examined the latency following stimulation for the onset of processed (filtered, rectified, and averaged) EMG signals (Figure 2.11). This latency test could be used to demonstrate that fibers recruited through DRG stimulation were sensory afferents and not motor neurons in the VR; that is, that DRG stimulation did not result in current spread sufficient to activate VR fibers and confound our results. Following activation of a motor neuron by VR stimulation, this latency would depend on the conduction velocity of the recruited fiber and the distance between the stimulating electrode and the muscle from which an EMG was recorded. However, the latency following DRG stimulation would additionally depend on the transmission delay imposed by the

trans-synaptic activation within the spinal cord of a motor neuron by activated sensory neurons. Therefore, we expected that the latency to evoke an EMG response following VR stimulation would be approximately 1 ms less than the latency following DRG stimulation. Figure 2.11 shows that there was, in fact, no measurable difference in the latencies to recruit MG EMG via VR and DRG stimulation at the suprathreshold level of 50 μA, both with medians of 2.6 ms across 47 VR channels and 31 DRG channels. A Mann-Whitney U-test showed no significant difference in these distributions ($p = 0.03$). Note that noise in the EMG signal coupled with an insufficiently high EMG sampling rate may make it impossible to use this latency test as evidence for or against current spread being isolated to the VR or DRG (see discussion).

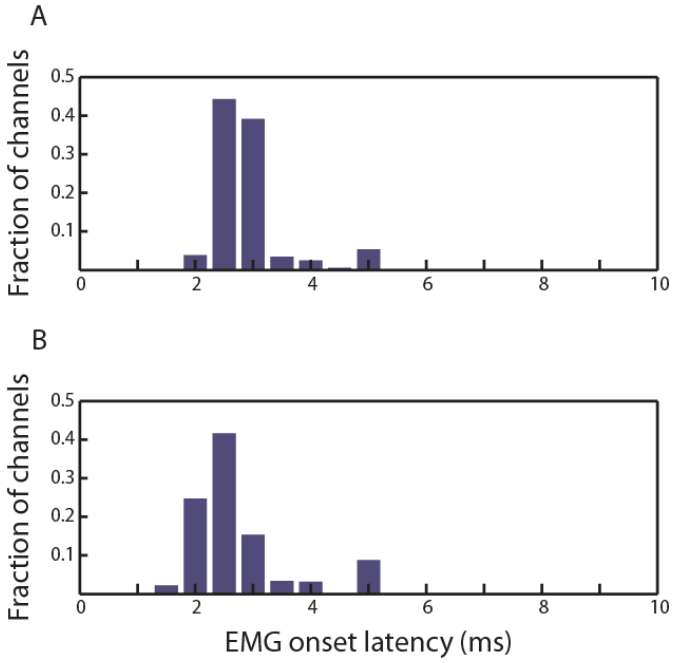

Figure 2.11 Distribution of latencies to onset of EMG response following stimulation. (A) VR stimulation produces EMG responses in the MG muscle with latencies of median 2.6 ms at 50 μA. (B) DRG stimulation produces MG EMG responses that are not significantly different from those of VR stimulation under the same stimulus conditions (Mann-Whitney U-test, $p = 0.03$). These data are taken from all 47 VR channels and 34 DRG channels across frequencies for EMG recorded from the MG muscle.

We then performed a similar analysis, measuring the latencies for onset of force following stimulation in VR or DRG (Figure 2.12). While the latency measure did not provide additional insight about current spread and resulting fiber recruitment, Figure 2.12A shows some interesting differences between VR and DRG stimulation. Forces are plotted versus time for those VR and DRG channels whose force responses exceeded baseline. For the stimulus amplitude tested – 30 μA – stimulation on several DRG channels demonstrated greater force magnitudes than stimulation on VR channels. We would expect that, if DRG stimulation resulted in current spread to the VR, then the forces produced by DRG stimulation should generally be *smaller* than those produced by VR stimulation. It is unlikely that at such a low current amplitude, current spread from the DRG would generate larger forces than direct VR stimulation at that same amplitude.

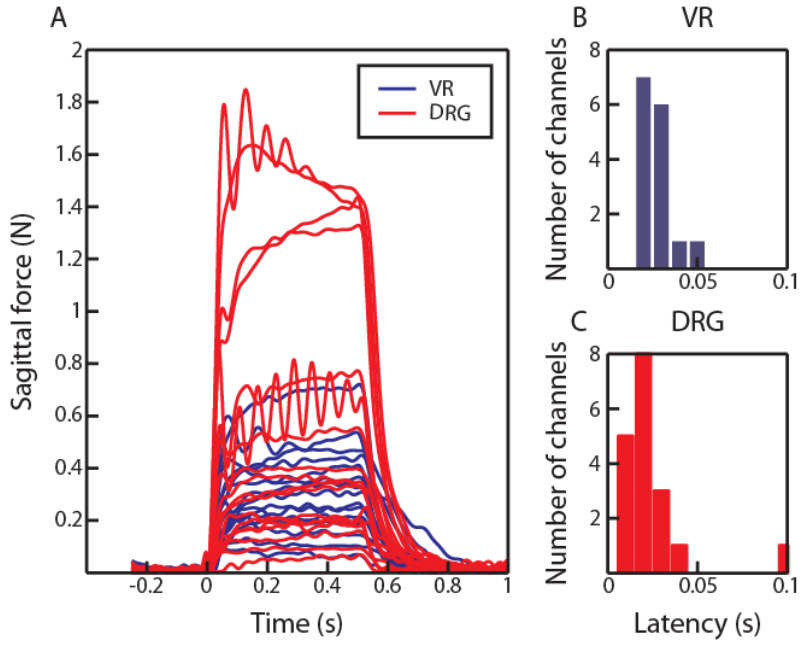

Figure 2.12 Latencies to onset of force following VR or DRG stimulation. (A) Force versus time for stimulus channels whose forces exceeded baseline in response to VR stimulation (blue) and DRG stimulation (red). (B) VR stimulation at 30 μA and 50 Hz produces force responses with latencies of median 20 ms. (C) DRG stimulation produces force responses that are not significantly different from those of VR stimulation under the same stimulus conditions. These data are taken from the 15 VR channels and 18 DRG channels whose forces were larger than baseline for these stimulus conditions.

2.4 DISCUSSION

Previous work has not explored the possibility of stimulating the VR or DRG for restoring motor function to treat paralysis. In these experiments, we measured EMG and endpoint force in response to VR or DRG stimulation to characterize these responses as a function of stimulus amplitude, frequency and implant location. This analysis represents a first step in evaluating the performance of a potential new interface for use in FES systems.

2.4.1 Frequency dependence

We noted that both the EMG and force waveforms comprised an initial transitional phase followed by a steady state response to the stimulus pulse trains. The steady state was the response component in which we were most interested because it represented constant muscle contraction, which is useful for voluntary, sustained movements. As we increased the stimulus frequency to 300 Hz in rats, the steady state response was markedly diminished, as if the system were acting as a low pass filter. Typically, motor neurons fire at less than 20 Hz, with force output being in part a function of motor neuron firing rate [38]. Indeed, studies have shown that cat [39, 40] and human [41] muscles do behave as second order low pass filters with cutoff frequencies of 20 – 30 Hz. However, Baldwin and colleagues reported that tibial nerve and triceps surae stimulation at 100 Hz could produce significantly more torque than at 20 Hz [42]. The authors suggest that high frequency afferent stimulation, resulting in trans-synaptic activation of motoneurons with larger, consistent contractions, be explored for use in FES. Stimulus frequencies greater than 100 Hz were not tested, and could represent a limit for this stimulus parameter.

It was interesting to note that DRG stimulation had a similar frequency dependency to VR stimulation, even though the mechanism for evoking muscle activation is indirect. For DRG stimulation, we originally hypothesized that larger stimulus frequencies would be beneficial because a motor neuron receiving synaptic input from an afferent stimulated at high frequency would be more likely to fire due to integration of the high-frequency synaptic activity. However, over the range of frequencies tested, we did not observe a benefit of increased stimulus frequency on motor response in comparison to VR stimulation. Future experiments would require finer variation of frequency as a stimulus parameter to explore these frequency effects.

2.4.2 Power consumption and selectivity for target muscle

Next, we examined EMG activity to observe the distributions of thresholds. The thresholds for VR stimulation were quite low with a narrow distribution about a median of approximately 12 μA. These thresholds were comparable to those found for IFMS [24, 25, 34, 36]. They were only slightly larger than the 5 – 10 μA reported for VR stimulation [32] or 5 μA reported for human intraneural stimulation [43]. DRG stimulation, on the other hand, demonstrated a broader distribution of thresholds about a larger median of approximately 25 μA. This distribution is not unlike those observed for ISMS [16, 44-47]. This broad distribution of thresholds for DRG stimulation may be due to the heterogeneity of the tissue; it not only contains fibers of passage, but also cell bodies. A stimulating electrode may be close to a group of fibers, resulting in a low threshold, or it may be close to a cell body, resulting in a high threshold (see chapter 4). It should be noted that isoflurane is known to suppress activity of neurons in the spinal cord [48-50]. This suppression could provide an obstacle to trans-synaptic activation of motoneurons, resulting in the increased thresholds for DRG stimulation that we observed. It is also possible that at these

higher stimulus amplitudes, current spread invaded the VR, resulting in motor neuron recruitment rather than sensory afferent recruitment, as discussed above.

After establishing the thresholds for eliciting responses in the EMG, we further explored responses for which muscles were being activated at threshold. Both VR and DRG interfaces offered access to each of the muscles from which we recorded EMG. Ignoring channels in which antagonist muscle groups were both activated at threshold, there were differences between which muscles were recruited as a function of spinal level (i.e. L5 versus L6). Likewise, there were some differences between VR and DRG stimulation, especially where stimulation in DRG L6 seldom produced activation of TA at threshold. It is likely that the distributions of muscles activated in response to VR stimulation are directly proportional to the quantitative distribution of motoneurons in the VR innervating these muscles. It is uncertain if these distributions of muscles activated in response to DRG stimulation are, similar to VR stimulation, proportional to the distributions of sensory afferents innervating these muscles.

We then measured the difference in current amplitude between the threshold to recruit a muscle and the threshold to recruit its antagonist group. We used this metric to describe the interface's selectivity for a target muscle. Approximately 10% of VR stimulus channels and 20% of DRG stimulus channels demonstrated no difference in these current levels (Figure 2.6 C and D); that is, at threshold, a muscle group and its antagonist muscle group were both activated simultaneously. However, in approximately 20% of VR and DRG channels, there was a difference of up to 20 μA between the threshold to activate a muscle group and the threshold to activate its antagonist muscle group. There was no significant difference between these curves for VR and DRG stimulation; both VR and DRG stimulation demonstrated selectivity in the form of large differences between the thresholds to activate mutual antagonist muscles. Because

both interfaces demonstrated access to each muscle group at threshold, it is difficult to draw conclusions about the comparative performance of the two interfaces with this metric.

Both IFMS and ISMS studies usually report joint or endpoint kinematics instead of muscle recruitment, but both have demonstrated access to varied hindlimb muscles [24, 51]. This finding is not unexpected for IFMS because the electrodes are implanted distally, in peripheral nerves through which all the neurons supplying a target muscle course. In addition, selectivity is usually measured, in the case of IFMS, for a target fascicle [24, 25]. ISMS selectivity has been shown for muscle [44], but is evaluated on the interface's ability to target motoneuron pools in the spinal cord [5, 44, 45]. Therefore, it is difficult to compare our selectivity metrics with those previously published for other interfaces.

For our final EMG analysis, we examined patterns of combined muscle recruitment as measured by the muscles activated at threshold. Both VR and DRG stimulation demonstrated simultaneous activation of antagonist pairs of muscles in a small number of stimulus channels at threshold levels. However, many stimulus channels activated muscles at threshold levels that would result in useful trajectories. While VR stimulation represented a variety of joint actuation combinations, DRG stimulation almost exclusively resulted in a combination of ankle extension with knee flexion. We assume that VR stimulation produces motor responses in direct proportion to the distribution of motoneurons in the VR. Because DRG stimulation results in a similar but exaggerated distribution of muscle activation patterns, it is either due to (1) a different distribution of afferents in the DRG in comparison to their efferent counterparts in the corresponding VR, or (2) DRG stimulation taking advantage of spinal cord circuitry, which provides access to complex reflexive movements in response to activation of muscle afferents. Furthermore, we are unable to assume which types and quantity of afferents are required to

activate trans-synaptically a motor efferent innervating a particular muscle. Knowledge of the distributions of neurons by target of innervation in these tissues would help us understand this mechanism (see appendix B).

2.4.3 Force recruitment curves and vectors

After analyzing the EMG responses, we turned our attention to the endpoint force responses to stimulation. The recruitment curves were roughly linear with no significant difference between VR and DRG recruitment rates of approximately 0.015 N/μA. Both interfaces demonstrated the capacity for controlled, graded force recruitment over the stimulus amplitudes tested. The broad distribution of DRG stimulation thresholds may have led us to expect more gradual force recruitment than VR stimulation with its lower thresholds, but these two metrics – threshold and force recruitment rate – are not equivalent. As mentioned, the heterogeneity of the DRG results in the possibility that a DRG stimulating electrode will be near a cell body, which would influence the threshold. However, in either tissue, once stimulation reaches threshold, they appear to recruit force at the same rate.

Forces of up to 1 N were achieved in response to VR stimulation and almost 2 N of force were recorded on some channels in response to DRG stimulation. These forces are comparable to those recorded in response to ISMS in rats [52]. The recruitment curves were approximately linear and demonstrated graded force recruitment. We observed that the slopes of the recruitment curves resulting from VR stimulation and DRG stimulation were similar (Figure 2.8). However, we were unable to make direct qualitative comparisons to either IFMS or ISMS. Normann and colleagues [34] demonstrated recruitment curves for IFMS, but those were measured specifically for gastrocnemius force, not endpoint force. Likewise, Bamford and colleagues [26] reported

recruitment curves for ISMS that were far broader than for nerve cuff stimulation, but these curves were plotted against normalized quadriceps force. It is worth noting that for most stimulation channels, the forces measured did not reach a maximum at 100 μA stimulation, which was the maximum amplitude limit for our stimulator. We might have measured larger endpoint forces had we been able to continue increasing the stimulus intensity. Finally, we plotted the force vectors in the sagittal plane. At twice EMG threshold, the limb predominantly exhibited caudal extension. There was little difference in the directions between VR and DRG stimulation. Tresch and colleagues [52] plotted endpoint direction as a function of location along the spinal column in response to ISMS in rats. The directions that they reported at the L5 to L6 levels were similar to those reported here. Stimulation at more rostral spinal levels, or caudally at S1, would likely produce vectors that are different in direction from those observed here.

2.4.4 Response onset latencies

When implanting the DRG or VR for stimulation with a single wire electrode, we should not take for granted that the current spread is isolated to that tissue. For these experiments, we used a micromanipulator to control the depth of the electrode as it penetrated the DRG, never going deeper than half the width of the DRG, which was approximately 2 mm. Use of a surgical microscope gave us visual feedback of electrode implantation in the target tissue. We similarly implanted the VR. Thus, it was unlikely that we implanted an electrode into a location other than what we expected. However, even if the electrode is physically located in the target tissue, current may spread to other tissues and confound our results. When stimulating the VR, we performed a dorsal rhizotomy, cutting the dorsal root. This surgical measure ruled out the possibility of current spread to the DRG and potential afferent activation contributing to the

EMG and force results. In the case of DRG stimulation, ruling out the possibility that current spread lead to activation of efferents in the VR is more complicated.

First, we assumed that current was not likely spreading to the VR via DRG stimulation at the current amplitudes tested, due to the resistivity of the tissue. Investigators stimulating motor neurons in the cat spinal cord determined that the threshold to activate the fiber (I_{th}) was proportional to the squared distance to a node of Ranvier (r^2) by $I_{th} = kr^2$ [53, 54]. It is reasonable to assume that the resistivity of the DRG will be similar to that of the spinal cord because of a similar composition of cell bodies and fibers of passage. At 50 μA stimulation, we can expect to activate a fiber with a node of Ranvier up to approximately 600 μm away from the electrode. At 100 μA, this distance increases to approximately 1 mm [55]. Note that this is the distance to a node of Ranvier, *not* to a fiber, thus a fiber that is 1 mm away from the electrode is actually unlikely to be activated. Moreover, Grinberg and colleagues, when modeling the peripheral nerves of cats, noted that the resistance imposed by layers of perineurium was a non-trivial barrier to current spread [56]. Therefore, we assume that the barrier between the DRG and VR is also a non-trivial barrier to the spread of current from an electrode in the DRG to fibers in the VR that are at least 1.5 mm away.

Ultimately, we need objective, empirical evidence to determine if DRG stimulation at the current levels tested is indeed isolated to the DRG, rather than recruiting fibers in the VR. To this end, we measured the latencies to onset of EMG signals following stimulation in VR and DRG, but found no difference, with both latencies equal to approximately 2.6 ms (see Figure 2.11). We expected to see a 1 ms increase in latency for DRG stimulation to account for the extra synaptic delay [29]. Though our test did not detect a difference, it is possible that the low resolution of the EMG signal (0.4 ms) and the noise on the EMG signal make this method impractical for finding

a 1 ms difference in EMG onset latencies. It may also be possible that, through different mechanisms, DRG and VR stimulation would not have very different EMG onset latencies. We then examined the forces produced under the same stimulus conditions and found that several channels produced forces at least as large as or larger than VR stimulation (Figure 2.12). This result makes sense if we assume that DRG stimulation is activating afferents and generating forces through reflex pathways. However, if DRG stimulation were merely activating motor neurons through current spread to the nearby VR, then we would expect it to produce smaller forces under the same stimulus conditions than VR stimulation.

To test if DRG stimulation results in current spread that activates VR fibers, we must knock out the reflex pathways between the afferents in the dorsal roots and the efferents in the ventral roots. One simple method, though non-reversible, would be to cut the dorsal roots proximal to the stimulating electrode. As mentioned at the beginning of the results section of this chapter, we cut both dorsal and ventral roots proximally, and stimulation in the DRG resulted in no EMG response. However, it is possible that cutting those ventral roots rendered the motor neurons less likely to be activated. It may also be possible to use serotonin antagonists to shut down the trans-synaptic activation of efferents through afferent stimulation. Murray and colleagues used serotonin agonists and antagonists to evaluate which serotonin receptor subtypes influenced persistent calcium currents after spinal cord injury in an in vitro cat preparation of spinal cord and dorsal and ventral roots [57]. This method is useful because by using serotonin antagonists, we would have a reversible means of shutting down the trans-synaptic activation of efferents through afferent stimulation. If DRG stimulation still results in motor responses after we interrupt the reflex pathways, by either surgical or pharmacological means, then current spread is indeed causing activation of efferents in the nearby VR.

2.5 CONCLUSIONS

We compared VR stimulation to DRG stimulation, while in turn also comparing these to other interfaces. The thresholds were lower for VR stimulation than for DRG stimulation, though the difference is not so large that we should dismiss DRG stimulation. Both threshold distributions are an order of magnitude smaller than that of nerve cuff stimulation [15, 35]. This minimal power requirement is important for the design of a portable, battery-powered interface. In addition, VR and DRG stimulation demonstrated graded force recruitment, and both evoked functionally large hindlimb forces from single-channel stimulation. After comparing the performance of these interfaces, neither was inherently superior to the other, and both warrant further investigation.

In these experiments, we took the first steps toward evaluating the performance of two potential interfaces for use in FES systems. There were some limitations in our experiments that should be addressed in future work. First, we did not record contractile forces from individual muscles. Second, we did not have access to all motor neurons innervating a target muscle; we did not have a means to elicit maximal contractions from a muscle. An experiment where the focus was placed specifically on recruitment of tibialis anterior and gastrocnemius muscles could include instrumentation to measure muscle force as well as sciatic nerve cuff stimulation to produce and measure maximal force contractions. These data would allow for the measurement of force recruitment comparable to those reported for IFMS and ISMS. Finally, we did not test fatigue resistance for VR or DRG stimulation and future experiments should be designed to test the ability of these interfaces to maintain muscle contractions for extended durations. Given the findings presented here, both interfaces show promise for use in FES systems.

3.0 MOTOR RECRUITMENT IN RESPONSE TO VENTRAL ROOT OR DORSAL ROOT GANGLION MICROSTIMULATION IN CATS

In this chapter, we extend the work of the previous chapter, translating from the rat model to the cat model. We focused our analyses on the fixed endpoint forces resulting from DRG stimulation and in one cat from VR stimulation. Single channel microstimulation in the DRG produced force magnitudes and directions similar to those reported for ISMS. Analysis of these data provided further information for comparing the quality of VR or DRG stimulation to other interfaces, such as IFMS and ISMS.

3.1 INTRODUCTION

In our lab, we perform electrophysiology experiments in cats wherein we stimulate in the DRG to activate primary afferents for artificially introducing sensory information to the central nervous system. These experiments provided an opportunity to translate the rat experiments presented in the previous chapter to the feline model. There were two main advantages to adopting a feline model and continuing with our experimental design. First, the cat's VR, DRG and other structures are significantly larger, which allows us to use multielectrode arrays. The use of these arrays increases the number of stimulus channels available to us as well as the efficiency with which we can perform the experiment. Second, investigators typically choose the

cat model for electrophysiology experiments examining FES. We are therefore able to record force output in response to stimulation with our proposed interfaces and make appropriate comparisons to published data for other interfaces.

The experimental design is similar to that for rats, though limited because we were adapting to existing cat experiments. In this chapter, we focus on endpoint forces evoked in response to VR or DRG stimulation. In response to DRG stimulation, we found similar force magnitudes and directions as reported for ISMS at these spinal levels [16, 47]. In addition, the thresholds to evoke motor responses were similar to ISMS [30, 58]. As with the rat experiments, we found that the threshold to observe activity in response to VR stimulation were lower than for DRG stimulation. We conclude that (1) VR and DRG stimulation warrant further investigation as they perform comparably to other interfaces and (2) the cat model should be used to further investigate VR and DRG stimulation.

3.2 METHODS

This experiment was designed in similar fashion to that presented in chapter 2 for rats. Here we recorded fixed endpoint forces evoked by microstimulation in the feline VR or DRG. The surgical procedures provided access to the VR and DRG for stimulation. Stimulus amplitude and electrode location were varied in order to explore the effects of these parameters.

3.2.1 Surgical preparation

All procedures were approved by the Institutional Animal Care and Use Committee (IACUC) of the University of Pittsburgh. Experiments were conducted in four healthy adult cats (3 - 5 kg). Throughout the experiment, the subject's body temperature was maintained at 37 °C using an electric heating pad and a rectal thermometer. Under isoflurane anesthesia (1.5 - 2.5%), we performed a laminectomy to expose the spinal cord and spinal roots at the 6^{th} and 7^{th} lumbar segments (L6 and L7). Anaesthetic levels were maintained for cat 1 with a mix of alpha-chloralose and 0.5% isoflurane, for cat 2 with only isoflurane, for cat 3 with only isoflurane after decerebration, and for cat 4 with alpha-chloralose alone. While the maintenance dose for alpha-chloralose was 20 mg/kg, the initial dose was 70 mg/kg. These differences in anaesthetics across subjects were the result of constraints imposed by the cat preparations that we shared as part of the larger cat experiments. Following the laminectomy, we transferred the animal to a spinal frame with the torso supported and the hindlimbs allowed to move freely. The head was fixed in a stereotaxic frame and vertebrae clamps and hip pins were used to stabilize the spine. When stimulating in the VR, we additionally performed a dorsal rhizotomy to expose these roots. This rhizotomy helped visualize the VR for improving placement of the stimulating electrode in the VR and assured that responses to stimulation were not due to activation of spinal reflexes via the dorsal roots. At the end of the experiment, the animal was euthanized with a 5 mg/kg dose of potassium chloride.

3.2.2 Stimulation and data acquisition

We implanted electrodes for electrical microstimulation into the exposed VR or DRG. In the DRG, we implanted microelectrode arrays with 400 μm interelectrode spacing and shank length of 1.5 mm (Blackrock Microsystems, Salt Lake City, UT); we inserted a 4 x 10 array into the L6 DRG and a 5 x 10 array into the L7 DRG. These activated iridium arrays had impedances of approximately 50 - 100 kΩ at 1 kHz. For VR stimulation, we implanted a linear microelectrode array with 4 shanks and 4 electrode sites per shank, for a total of 16 electrode sites (MicroProbes, Gaithersburg, MD). Activated Pt/Ir electrode sites were 50 μm in diameter and 500 μm apart on shanks approximately 200 μm in diameter, with impedances of approximately 0.1 MΩ at 1 kHz. A stainless steel wire placed in the epidural space along the spinal cord acted as the return electrode. Stimulus waveforms were generated and delivered using an RX7 microstimulation system (Tucker-Davis Technologies, Alachua, FL). These waveforms were biphasic and charge-balanced, with a cathodic-leading 200 μs pulse followed by a 400 μs anodic pulse. Stimuli were delivered in 500 ms trains at frequencies of 10 – 1000 Hz and at amplitudes of 1-100 μA (cathodic phase). Stimulus repetitions (n = 5), amplitude and channel were randomized and all stimulation was single-channel. In cat 1, we tested frequencies of 10, 50, 100, 300 and 1000 Hz. In cats 2 and 3 we tested frequencies of 50 and 100 Hz, and in cat 4 we tested frequencies of 30, 60 and 100 Hz. Variance in stimulus frequencies across subjects was due to (1) constraints from sharing cat preparations and associated DRG stimulation data and (2) an effort to adapt stimulus parameters to explore stimulus frequency dependence on force generation.

The animal's foot was mounted to an insulated aluminum rod that was attached to a rigidly fixed six-axis force transducer (ATI, Apex, NC). This force transducer recorded the fixed

endpoint force of the ipsilateral hindlimb in response to microstimulation. Force data were recorded at 1 kHz using a custom-built LabVIEW program (National Instruments, Austin, TX). A transformation matrix was applied to these data to correct for three-dimensional angle and displacement differences between the location of the animal's foot at the end of the rod and the location of the force transducer.

3.2.3 Data analysis

Using a 4^{th} order Butterworth lowpass filter, force data were smoothed with a cutoff frequency of 20 Hz. These data were rectified, aligned to the beginning of each stimulus pulse train and averaged. We defined threshold as the stimulus amplitude that resulted in a mean force greater than the mean plus two standard deviations of baseline force. Above this cutoff level, there is only a 5% chance that signals are indistinguishable from background noise. We then estimated the slope of the recruitment curve using linear regression from the threshold to the amplitude at which 75% of maximum recruitment was achieved. Finally, we calculated the magnitude and direction of the averaged force responses.

3.3 RESULTS

The primary aim of these electrophysiology experiments was to examine the force responses in the hindlimb to microstimulation in the feline lumbar VR or DRG and then evaluate the potential quality of these interfaces. The stimulus amplitude and electrode location were varied to examine their effects on recruitment of fixed endpoint forces. Table 3.1 summarizes the quantities and

locations of the stimulus channels on which we stimulated. Note that the linear microelectrode array was only available for VR stimulation in cat 4.

Table 3.1 Number of stimulus channels across cats and stimulation sites. Four cats and two stimulation sites were tested. All stimulation was single-channel.

	Cat 1	Cat 2	Cat 3	Cat 4
VR L6	0	0	0	7
VR L7	0	0	0	8
DRG L6	12	18	10	10
DRG L7	10	1	14	13

Figure 3.1 shows a typical force waveform and recruitment curve for evoking endpoint force in response to DRG stimulation in cat. The time-dependent force waveform demonstrates the same pattern shown in rat (Figure 2.7), which includes an initial transitional phase followed by a steady state that begins at approximately 200 ms and continues until the end of stimulation. The recruitment curve is approximately linear, a property that was consistent for most of the responding channels.

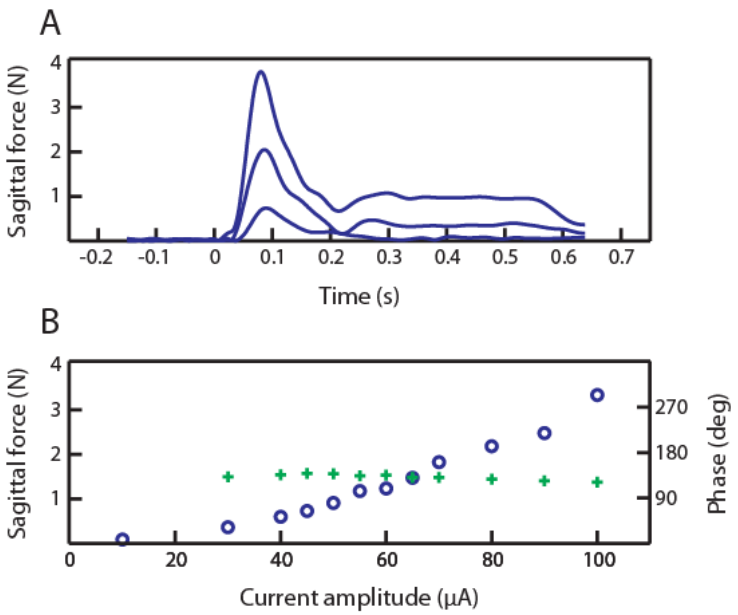

Figure 3.1 Force waveform and recruitment curve in response to feline DRG stimulation. (A) Typical force waveform in response to stimulation at 100 Hz and 40, 70 and 100 μA on DRG channel 10 of cat 2. (B) Recruitment curve for the same channel as stimulus amplitude is increased. Circles denote force magnitude and plus signs (+) denote direction; note the consistent force direction.

However, in approximately 12% of responding channels, the recruitment curve looked typical until sufficiently large stimulus amplitudes were used, usually at least 70 μA, at which point the endpoint forces increased dramatically (Figure 3.2). The direction of the endpoint force also changed significantly. We did not observe this phenomenon in rats or in response to VR stimulation in cat 4, and accurate measurement of the magnitude or direction of these forces was not possible because they were beyond the limits of the force transducer.

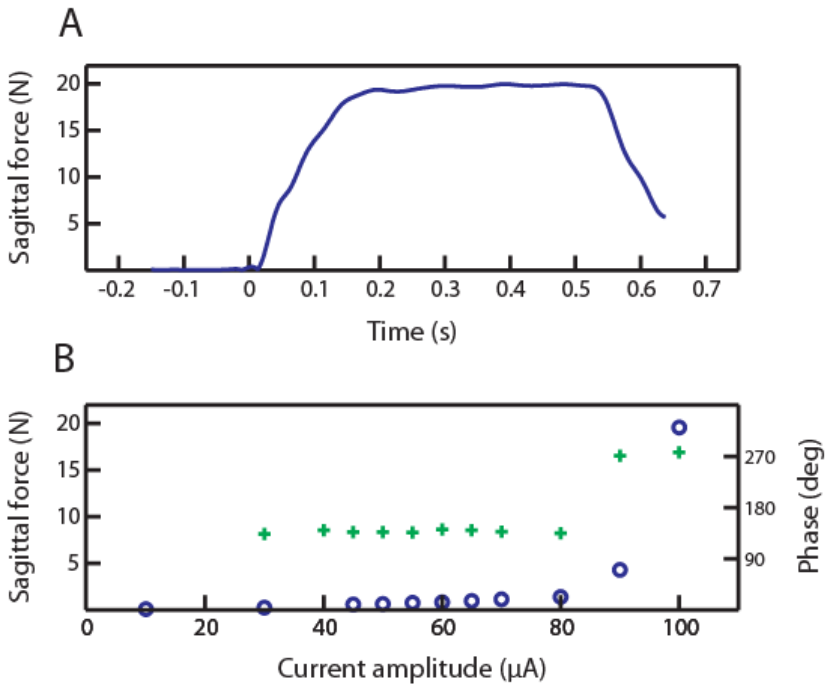

Figure 3.2 Some DRG channels produce significantly increased forces. For some stimulus channels, force waveform reached limit of force transducer. (A) Force waveform in response to stimulation at 100 μA and 100 Hz on DRG channel 26 of cat 2. (B) Recruitment curve for the same channel as stimulus amplitude is increased. Circles denote force magnitude and plus signs (+) denote direction; note the consistent force direction. As the stimulus intensity increased beyond 80 μA, the force magnitude increased dramatically and the direction changed significantly.

Next, we examined the distribution of thresholds and recruitment curve slopes for the different subjects. The data used for these comparisons were taken across VR and DRG channels for stimulus frequencies between 30 and 100 Hz; there was no stimulus frequency dependency for the recruitment slopes or thresholds to detect force. However, there was a significant difference in the thresholds for these subjects (Figure 3.3). Cats 1 and 3 had lower thresholds to generate endpoint forces than cats 2 and 4 for DRG stimulation. In addition, the thresholds to generate force in cat 4 were lower for VR stimulation then DRG stimulation, which is consistent with what we observed in rats (see chapter 2).

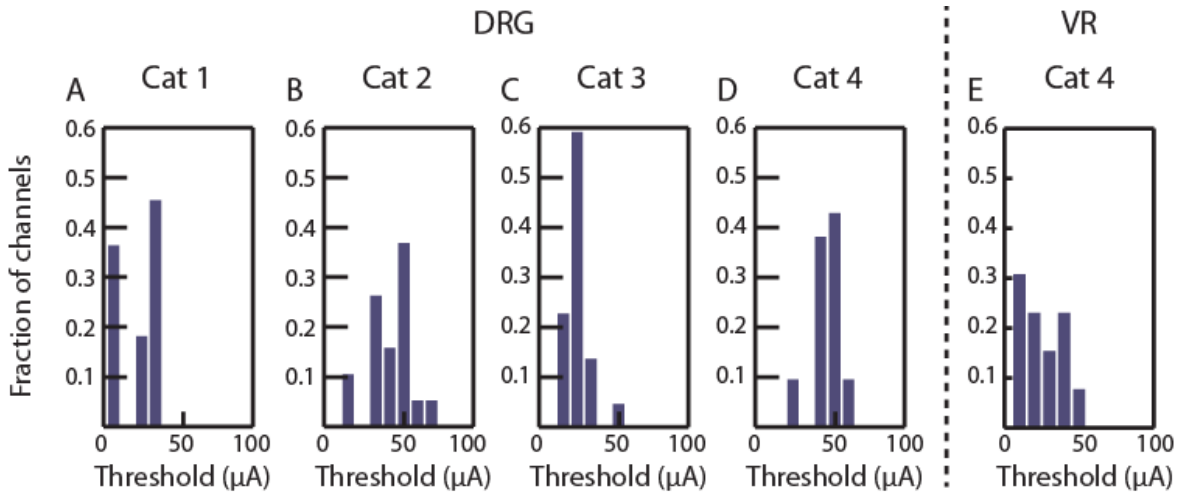

Figure 3.3 Distribution of thresholds to generate force in response to VR or DRG stimulation in cats. (A-D) Distribution of thresholds in response to DRG stimulation in cats 1 – 4. Cats 1 and 3 demonstrated significantly smaller thresholds to measure forces than did cats 2 and 4. (E) Distribution of thresholds in response to VR stimulation in cat 4. The threshold for VR stimulation was lower than for DRG stimulation in cat 4. Data were taken from all DRG and VR channels in all cats at stimulus frequencies between 30 and 100 Hz. These results are consistent with those found in rat.

With the exception of cat 1, there was no significant difference in the slopes of the recruitment curves in response to DRG stimulation, with an average of approximately 0.03 N/μA (Figure 3.4 A-D). The mean slope observed from cat 1 was significantly larger than that of the other subjects, with a mean of approximately 0.1 N/μA ($p < 0.01$). Thus, cats 2, 3, and 4 demonstrated controlled, graded force recruitment in response to DRG stimulation.

Figure 3.4 E shows the distribution of slopes in response to VR stimulation in cat 4. There was no significant difference in recruitment between VR and DRG stimulation in this cat, which is consistent with observations for force recruitment in rat. Both interfaces demonstrated a capacity for generating graded force recruitment.

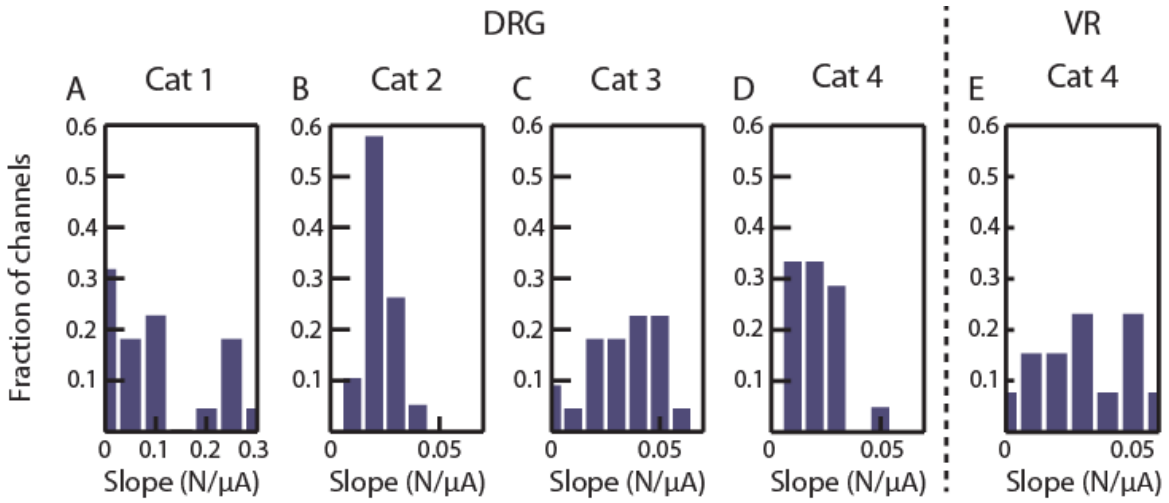

Figure 3.4 Distribution of force recruitment slopes in response to VR or DRG stimulation in cats. (A-D) Distribution of recruitment curve slopes in response to DRG stimulation in cats 1 – 4. Cats 2 – 4 had similar slopes, but cat 1 demonstrated significantly larger slopes; that is, cats 2 – 4 showed more graded force recruitment. (E) Distribution of recruitment curve slopes in response to VR stimulation in cat 4. There was no significant difference between the slopes for force recruitment in response to VR or DRG stimulation in cat 4. Data were taken from all DRG and VR channels in all cats at stimulus frequencies between 30 and 100 Hz. These results are consistent with those found in rat.

Finally, we calculated the magnitudes and directions of the force vectors for each cat, stimulus channel and stimulus condition, plotting them by implant location (Figure 3.5 and Figure 3.6). The plots in the top row represent the largest force magnitudes in the sagittal plane evoked by stimulation in each L6 DRG channel; likewise, the second row represents the maximum sagittal force output from stimulation in each L7 DRG channel. These plots demonstrate the range of directions of the force vectors, given implant location. There are low-magnitude vertical vectors as if the cat is lifting its foot. Predominantly, there are strong extension vectors directed vertically and posteriorly. There does not appear to be a consistent difference between the vectors resulting from DRG L6 stimulation versus DRG L7 stimulation. However, because the force output from the feline hindlimb overcame the limits of the force transducer (e.g. approximately -20 N in the vertical direction), we were unable to measure reliably the extreme force outputs for many of these trials.

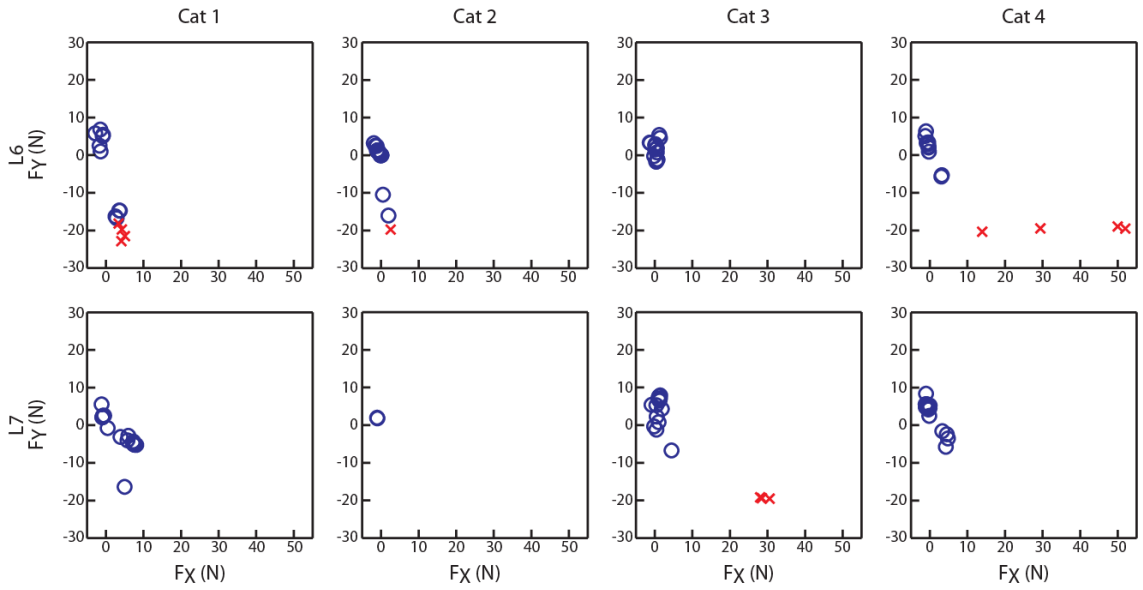

Figure 3.5 Maximum force vectors evoked by DRG stimulation in cats. Each stimulus channel is represented with the maximum force that stimulation on that channel produced in the sagittal plane. Negative Y forces represent the downward direction and negative X forces represent the rostral direction. There is no discernable difference in force directions between stimulation in L6 (top row) and L7 (bottom row). In all cats, forces in excess of the limit of the force transducer (-20 N vertical) were achieved; these forces are denoted as red X's.

VR stimulation in cat 4 produced similar forces as those from DRG stimulation (Figure 3.6). In addition, the directions were the same, with leg extensions directed vertically downward and posteriorly. However, no VR channels demonstrated very large forces that maxed out the force transducer, as was seen in some DRG channels. All force data reported here were for single-channel stimulation. As with rats, single-channel VR or DRG stimulation demonstrated the capacity to generate functionally large forces.

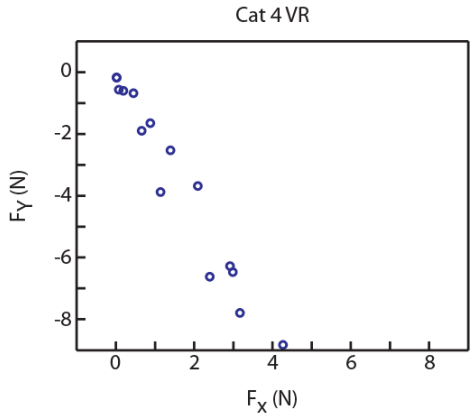

Figure 3.6 Maximum force vectors evoked by VR stimulation in cat 4. These data points represent the maximum force generated for each of the 15 VR channels in cat 4 across stimulus frequencies of 50 and 100 Hz. Negative Y forces represent the downward direction and negative X forces represent the rostral direction. VR stimulation in L6 and L7 produced caudal leg extension.

3.4 DISCUSSION

The previous chapter introduced experiments for stimulating the VR or DRG to evoke motor responses in rats. In the cat experiments presented in this chapter, we measured fixed endpoint forces in response to VR or DRG stimulation to characterize these responses as a function of stimulus amplitude and implant location. With the cat model, we were able to employ multi-electrode arrays for more efficient and higher throughput data collection. In addition, we can compare our feline force data to data published by other investigators for cats. We typically measured forces in excess of 1 – 2 N in response to DRG stimulation at amplitudes of up to 100 μA, which is similar to values reported by Lemay and Grill in response to ISMS in cats [16]. However, larger force magnitudes, capable of supporting at least half body weight, were reported by Saigal and colleagues in response to ISMS in cats [47]. They achieved forces of up to 20 N at approximately 80 – 100 μA. In our feline experiments, approximately 12% of stimulus channels,

increasing the stimulus amplitude beyond 80 μA resulted in dramatically increased endpoint forces of at least 20 N. Because our force transducer was limited in the vertical direction to approximately 20 N, however, we were unable to accurately measure these larger force vectors produced. In addition, we do not know why 12% of DRG channels produced these larger forces when this phenomenon was not observed in the other channels, or in VR stimulation or in any rat stimulation data. This result may be due to the activation of a strong extensor reflex or variable anaesthetic levels. Further work and data is needed to understand this result.

The thresholds, with the exception of cat 1, were the same for DRG stimulation across cats. VR stimulation in cat 4, however, required less current to generate forces than DRG stimulation. This decreased threshold for VR stimulation was consistent with data reported for rats in chapter 2. For both interfaces, the recruitment curves were approximately linear and, with small slopes, demonstrated graded force recruitment. While stimulation in rats recruited force at approximately 0.015 N/μA (see chapter 2), stimulation in cats recruited force at twice that rate. This larger rate is not surprising because cats can generate much larger forces than rats.

Finally, we plotted the force vectors in the sagittal plane. There was little difference observed in the directions of the endpoint vectors between DRG stimulation in L6 or L7. Stimulation in both ganglia produced caudal extension of the hindlimb as in rats. VR stimulation in cats likewise produces caudal extension at the spinal levels tested, with similar force magnitudes. We did not observe VR channels that produced very large forces as we did with some of the DRG channels, but we only tested 15 VR channels. It is important to note that these forces were generated in response to single-channel stimulation. Multi-channel stimulation may produce larger forces for completing motor tasks such as standing and walking.

3.5 CONCLUSIONS

We translated the rat experiments, discussed in chapter 2, to a cat model. We found that the comparisons between VR and DRG stimulation for threshold, recruitment curve slope, and force vector direction were consistent with results reported for rat in chapter 2. This change to a feline model allowed us to make additional comparisons to other interfaces because cats are typically the animal model chosen for these experiments in FES interfaces. We found similar forces and thresholds for DRG stimulation as those reported for ISMS. In addition, we were able to utilize multi-electrode arrays because the DRG are larger in cat than rat, which afforded us more stimulus channels and a more efficient experiment. In the cat experiments, we were able to examine single-channel stimulation across many channels, but we were not prepared to analyze data online. Had we been able to do this online analysis, we could have categorized stimulus channels by the forces they produced, and then combine these channels for multi-channel stimulation. This cat model would allow us to test different channel combinations in an effort to produce more force or change the direction of the force vector produced. Future work should continue to use the cat model and explore multi-channel stimulation.

4.0 NEURONAL RECRUITMENT IN RESPONSE TO MICROSTIMULATION IN VENTRAL ROOT OR DORSAL ROOT GANGLION

To address specific aim 2, we developed a computational model that estimates the number and sizes of fibers recruited in response to extracellular stimulation of the VR or DRG. This work provides insight into the mechanisms by which functional responses, as described in the previous chapter, might be produced. In addition, the model in its own right provides a tool with applications beyond those of this dissertation.

4.1 INTRODUCTION

In the previous chapter, we examined the EMG and force responses to stimulation in the VR and DRG. Those experiments characterized functional responses. However, electrophysiological methods are limited in their capacity to address questions such as those regarding the activation of individual neuronal fibers within a population. This method is not appropriate for examining the activity within the local volume around an electrode, the volume that is affected by electrical stimulation, to in turn understand the performance of an electrical interface. A computational model was a logical choice for an additional tool to study VR or DRG stimulation as potential FES interfaces as it overcomes these challenges.

Computational models have provided valuable insight into the effects of electrical stimulation on fiber recruitment in peripheral nerves. Veltink and colleagues [59] developed a model that simulated peripheral nerve geometries and conductivities, and then applied electric fields corresponding to stimulation. They used the McNeal model [60] for nerve fiber excitation to determine the neural response to stimulation and concluded that intraneural or even IFMS was necessary to selectively stimulate fascicles below the surface of a peripheral nerve. Subsequent work by [22, 23, 61], however, has shown that stimulus current steering methods and nerve reshaping can be used to increase selectivity for even deep fascicles, though there still exist limitations in activating smaller diameter fibers. Meier and colleagues [62] modeled electric field distributions in a nerve bundle and the response of single nerve fibers to arbitrary electric fields. They used these models to predict the response of bundles of peripheral nerve fibers to electric fields created from either monopolar or tripolar intrafascicular electrode configurations and found that tripolar stimulation achieved better spatial selectivity and yielded a more physiologically appropriate recruitment order. Recently, Butson and colleagues [63] used fascicular organization data from sciatic nerve slices to build a model for simulating intraneural stimulation of a sciatic nerve fascicle. The focus of that work was to examine recruitment as a function of electrode position and stimulation paradigm. They explored such factors as the current density within axons of different sizes, myelination as a barrier to fiber activation, and the spacing between electrode sites of a microelectrode array.

The models developed in these previous studies were based on specific geometries for the fiber bundles and do not generalize easily to other structures. In particular, the irregular and variable arrangement of fibers and cell bodies in the DRG makes it impractical to define a specific geometry to model the various electrode-fiber configurations that are possible. An

alternative approach, which has been used for modeling the recruitment of fibers by deep brain stimulation, is to estimate the volume of tissue activated (VTA) by a given stimulus current [64, 65]. Those investigators determined the VTA for a stimulus based on which neuronal fibers around an electrode were activated in response to that stimulus. A larger VTA meant that neurons further away from the electrode had been activated.

We used a similar approach to predict the activation of primary afferent fibers of various sizes as a function of stimulus intensity. We started by estimating the current-distance relationship, which determines the activation threshold as a function of the distance between the current source and nearest node of Ranvier. This distance then defines a volume around the electrode, which we term the volume of influence (VoI). Our model simplifies the electric field calculation by assuming a homogeneous, isotropic extracellular medium in a local volume surrounding the electrode, similar to the approach taken in McIntyre and Grill [31]. We adapted the multi-compartment neuron model in McIntyre and Grill [31] to determine the current-distance relationship for primary afferent neurons comprising a range of fiber diameters.

Given the assumption that the node of Ranvier is the site of activation, all fibers having a node within the VoI will be activated. Thus, a given stimulus will activate all fibers having at least one node within the boundary of the VoI. We used an analytical approach to determine the probability of finding a node of Ranvier inside the VoI. This probability depends on the internodal distance; smaller fibers have shorter internodal distances and therefore more nodes per unit length. It is not necessary to assume a specific electrode-node geometry because we integrate the probabilities over all possible configurations within the VoI (see appendix A for details). We implemented this ‘likelihood of activation’ approach to estimate the recruitment of primary afferent fibers by microstimulation in the VR or DRG. This approach assumes that the

distribution of fibers follows published data for the number and distribution of fibers of various diameters in these tissues. Given the current-distance relationship for each fiber diameter, the model provides a likelihood estimate of the number and types of fibers recruited based on the density and distribution of fibers by size. These features lead to a flexible model that can simulate various stimulation scenarios and electrode-fiber geometries, including the inhomogeneous distribution of fibers in the DRG. We have written a journal article that has been accepted for publication, which presents results using this computational model to simulate fiber recruitment in response to feline DRG stimulation [66].

4.2 METHODS

The computational model was developed in two parts. In the first part we simulated activation of single axons by a point source current using NEURON [67]. This single-fiber model was used to determine the current-distance relationships of primary afferent fibers having diameters in the range 7.3 – 16 μm. These current-distance relationships predict, for a given stimulus intensity and fiber size, the maximum distance an electrode can be from a node of Ranvier and still activate that fiber. In the second part of the model, we used the predictions from the current-distance relationships to estimate the likelihood of recruiting specific numbers of fibers of a given size within a normative population of DRG neurons. The population model was based on published data for the distribution of fiber sizes in feline L7 DRG [68].

4.2.1 Single-fiber model

Electrical excitability for a single fiber was represented with the double cable model published by McIntyre, Richardson and Grill, referred to as the MRG model and built in the NEURON environment [55]. Although cell bodies are present in the DRG tissue, we assumed that they were not directly excitable in the range of low amplitude (0 – 6 μA) stimulation currents that were simulated and so did not include them in our single-fiber model (see discussion). This single-fiber model uses

$$V_x = \frac{I*\rho_{ext}}{4\pi d_x}, \quad (1)$$

taken from [31] to describe the extracellular potential (V_x) acting on the fiber. Equation (1) is evaluated at each discrete compartmental location (x) along the length of the multi-compartmental fiber model to determine if, taken over the entire length of the fiber, the stimulus was sufficient to evoke an action potential in the simulated fiber. This expression is a function of the distance between the stimulating electrode and the segment of the fiber (d_x) as well as the current amplitude (I) applied through the resistivity of the extracellular medium (ρ_{ext}). This current-distance relation was computed for fibers of various discrete diameters (see Table 4.1). These fiber sizes were then included in simulations of heterogeneous populations of fibers.

While the MRG model was validated originally for peripheral motor axons, we used the model to predict activation of sensory fibers in this paper. Although studies have demonstrated that there are differences in the excitability of motor fibers and sensory fibers as a function of stimulus pulsewidth [69-71], Erlanger and Blair [72] showed that the difference was insignificant

at pulsewidths near 200 μs. For these simulations, we used biphasic, charge-balanced stimulus waveforms (200 μs cathodal, 400 μs anodal phases).

We used the single-fiber model to determine the maximum distance a monopolar, point source electrode could be from a fiber's node of Ranvier and still elicit an action potential from that neuron, for a given stimulus current amplitude and fiber diameter. In addition, we assumed an isotropic homogeneous extracellular medium with ρ_{ext} equal to 500 Ω-cm [31]. This assumption leads to a spherical VoI, with the radius defined as that maximum distance of activation determined from the current distance relationship (Figure 4.1A). Note that this assumption of isotropy may have significantly affected our results. However, we ran additional simulations assuming anisotropy, with resistivity values published for spinal cord [73]. Using a longitudinal resistivity of 300 Ω-cm and a transverse resistivity of 1200 Ω-cm, we found similar results as when assuming isotropy (see discussion).

We used the MRG model to simulate eight discrete fiber sizes (see Table 4.1). For each fiber size, we used the single-fiber model to determine the extent of the VoI (i.e. the radius) given variations in the stimulus amplitude. The current-distance relationships for the different fibers were then used as inputs to a population model to examine the probability of recruitment in a normative population of axons in the DRG.

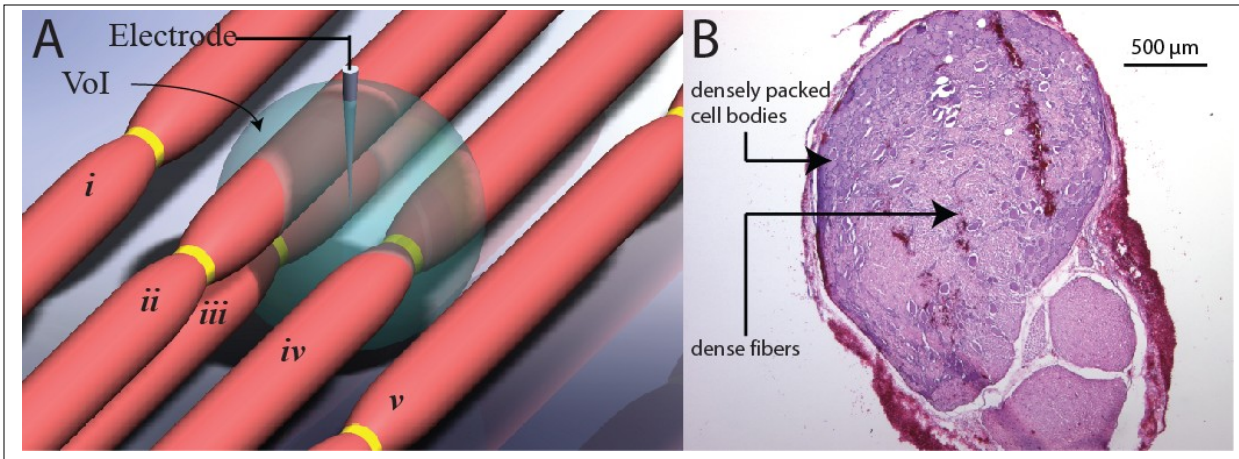

Figure 4.1 Sphere representing the volume of influence (VoI) created by a point-source current stimulus delivered by a microelectrode. (A) The radius of the sphere increases with stimulus amplitude and also varies with fiber diameter. The radius is determined by the current-distance relationship calculated with the single-fiber model for neuronal excitation. Fibers *iii* and *iv*, having a node of Ranvier within the VoI, will be activated. Fiber *ii*, though it passes through the sphere, does not have a node of Ranvier within the sphere and thus will not be activated. Fibers *i* and *v*, likewise, will not be activated. (B) Transverse section of feline L7 DRG (top) and VR (bottom), hematoxylin and eosin (H&E) stained. Cell bodies are predominantly located along the perimeter of the DRG, but are also sparsely distributed in the center among fibers of passage in the middle, which results in a heterogeneous tissue structure.

4.2.2 Population model

A computational model was developed in MATLAB (The Mathworks, Inc., Natick, MA) to determine the probability of recruiting a given number of fibers of a specified diameter, based on the likelihood of capturing a node of Ranvier within the VoI. This probability depends on two factors: 1) the density of axons packed in the VoI (i.e., the number of axons of a given diameter per cross-sectional area of the VoI), and 2) the inter-nodal distance of a given fiber diameter. In the simplest case, we could assume a uniform distribution of fibers in the DRG and compute the number of fibers of a given diameter packed in the VoI (N_{VoI}) to get

$$N_{VoI} = N_{fD} * \frac{A_{VoI}}{A_{DRG}}, \quad (2)$$

where N_{fD} is the total number of fibers of a particular fiber diameter (*fD*) present in the DRG and is based on published data of fiber distributions (see Table 4.1). A_{VoI} and A_{DRG} are the cross-sectional areas of the VoI and DRG tissue, respectively. For each fiber size, the radius of the VoI increases with the intensity of the stimulus current, and is taken from the current-distance relationship obtained with the single-fiber model. Note that in this work, we focus on the set of fiber sizes ($\{fD\}$) corresponding to medium and larger diameter fibers, representing the cutaneous and muscle afferent neurons that are the primary targets of stimulation in our studies. Equation (2) assumes that the fibers are distributed uniformly throughout the tissue. However, since the DRG is heterogeneous, containing a non-uniform distribution of fibers, cell bodies, and other tissue (Figure 4.1B), we modified (2) by

$$\boldsymbol{N_{VoI} = R_{DRG} * R_{fD} * \frac{A_{VoI}}{A_{fD}}}, \tag{3}$$

where the number of fibers having diameter *fD* passing through the VoI includes two additional scaling factors to account for the non-uniform distribution of fibers in the DRG. The first term, R_{DRG} represents the fraction of the VoI cross-section that is occupied by the fibers of interest, and we refer to this term as the *packing ratio*. The second term, R_{fD}, is the fractional fiber area and it represents the fraction of the fibers of interest comprising fibers of a specific diameter. A conceptual illustration of these parameters is provided in Figure 4.2. As shown in Figure 4.2B, only a portion of the VoI contains fibers of interest, due to the presence of other tissues (e.g. cell bodies, blood vessels, and smaller fibers).

Table 4.1 Model parameters for feline L7 DRG. For each fiber diameter included in the model, the table lists the number of fibers (N_{fD}) found in the feline L7 DRG based on (Risling, Aldskogius et al. 1983), as well as the fractional area of the fibers of interest occupied by each fiber size (R_{fD}), and the intermodal lengths (L_{int}) based on (Nilsson and Berthold 1988).

fD (μm)	7.3	8.7	10	11.5	12.8	14	15	16+
N_{fD}	1780	1730	1160	1920	1270	1370	630	990
R_{fD}	0.06	0.09	0.08	0.17	0.14	0.18	0.10	0.17
L_{int} (μm)	750	1000	1150	1250	1350	1400	1450	1500

An average value for the packing ratio (R_{DRG}) can be calculated based on fiber counts and cross sectional area for each of the fibers of interest, expressed as

$$\boldsymbol{R_{DRG}} = \frac{\sum_i N_{fD_i} * A_{fD_i}}{A_{DRG}}. \quad (4)$$

However, the actual value may vary substantially throughout the DRG, being higher in areas densely packed with fibers and lower in areas containing more cell bodies (see Figure 4.2B). To examine the effects of this variation on the model, we performed simulations to predict the probability of recruiting at least one fiber, varying the stimulus intensity from 1 – 6 μA and the packing ratio from 0.1 to 1.0. The simulation results were compared with recruitment threshold data from [74] to determine an appropriate range of values for R_{DRG} (see discussion).

Published data for the distribution of fibers of various sizes in the L7 dorsal roots of cats is provided in [68]. These data were used in

$$\boldsymbol{R_{fD}} = \frac{N_{fD} * A_{fD}}{\sum_i N_{fD_i} * A_{fD_i}} \quad (5)$$

to calculate the fractional area of the fibers of interest that is occupied by fibers of a specific diameter (R_{fD}; see Table 4.1 and

Figure 4.2B). Note that the data reported in [68] is for fibers in the dorsal roots. To account for the ~30% decrease in fiber diameter that occurs between the DRG and dorsal roots [75], we scaled the fiber diameters listed in the Risling data by a factor of 1.4 to represent fiber diameters in the DRG. For example, Risling found that there are approximately 1780 fibers in the dorsal roots with diameter equal to 5.1 μm, corresponding to the group of 7.3 μm fibers in the DRG (see Table 4.1). Lastly, we grouped all fibers having diameters equal to or greater than 16 μm into one group of "16+" μm fibers.

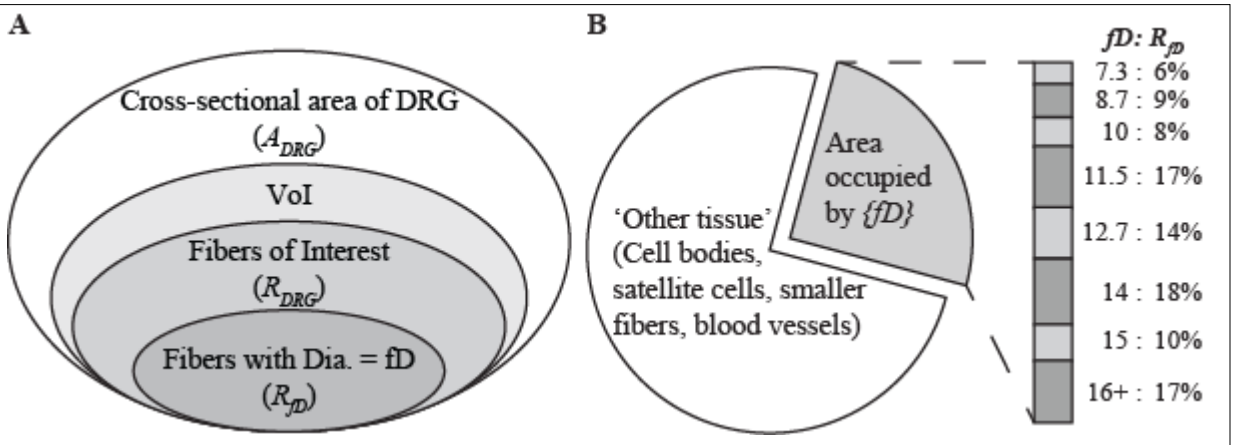

Figure 4.2 Conceptual illustration (not drawn to scale) of model parameters associated with the distribution of fibers in the VoI. (A) The VoI comprises a small portion of the total area of the DRG, a fraction of which is in turn composed of the fibers of interest (R_{DRG}). The area associated with fibers of interest is further divided into portions associated with specific fiber diameters (R_{fD}). (B) Pie chart illustrating fractional areas of DRG composed of 'other tissue' and the fibers of interest. The *packing ratio* comprises fiber diameters 7.3 μm and larger, each having a fractional fiber area (R_{fD}) based on the number of fibers of each diameter found in the DRG. The percent area associated with each fiber diameter is shown by the stacked bar plot at the right of the pie chart.

In (3), we estimated the number of fibers of a given diameter that pass through the VoI (N_{VoI}). This equation was evaluated for each specified fiber size, for a given stimulus amplitude. To determine which of these fibers would become activated, we must evaluate the probability of each fiber having a node of Ranvier within the boundary defined by the radius of the VoI (r_{VoI}). The probability that a fiber of a given diameter has a node of Ranvier within the VoI depends on

the ratio of the length of fiber captured by the VoI (L_f) over the internodal length of the fiber (L_{int}). If a fiber passes through the VoI at a known radial distance (r_f) from the center, the probability that a node is captured within the VoI is given by

$$P(node|I, fD, r_f) = \begin{cases} \frac{L_f}{L_{int}} = \frac{2\sqrt{r_{VoI}^2 - r_f^2}}{L_{int}} & L_{int} > 2r_{VoI} \\ \min\left(1, \frac{L_f}{L_{int}}\right) & L_{int} \leq 2r_{VoI} \end{cases}. \quad (6)$$

In cases in which the VoI is sufficiently large such that the length of the fiber encapsulated in the VoI is greater than the internodal length of the fiber, this equation would evaluate to 1. For example, a fiber passing through the center of a large VoI (i.e., $L_{int} < 2r_{VoI}$) will be guaranteed to have a node of Ranvier within the VoI. However, for stimulation intensities in the range 1 – 6 μA, the diameter of the VoI is ~40 – 240 μm. The range of internodal lengths for the fibers we examined was from 750 – 1500 μm, and thus (6) evaluates to much less than 1 at all values of r_f for this range of low intensity of stimuli.

Since the location of the fiber (r_f) is not known a priori, we computed an average value of the probability by integrating over all possible locations of the fiber within the VoI and normalizing by the cross sectional area of the VoI as shown in

$$P(node|I, fD, L_{int} > 2r_{VoI}) = \frac{\int_0^{rVoI} L_f * 2\pi r_f * dr_f}{L_{int} * \pi r_{VoI}^2}. \quad (7)$$

Equation (7) applies only when the diameter of the VoI is less than the internodal length of the specified fiber (i.e., at low current amplitudes), as is the case for the 1-6 μA range of stimulation current examined here. However, for a higher current amplitude that results in a VoI whose diameter is larger than the internodal length, (7) is insufficient and an alternate equation is required (see appendix A).

Next, the probability mass function for a binomial distribution is used to compute the probability of recruiting a given number of fibers of a particular diameter (N_{act}) from the number of fibers packed in the VoI (N_{VoI}) to get

$$\boldsymbol{P(N_{act}|I,fD) = \binom{N_{VoI}}{N_{act}} P(node|I,fD)^{N_{act}}[1 - P(node|I,fD)]^{N_{VoI}-N_{act}}.} \quad (8)$$

This calculation was performed for each fiber size and depends on the current amplitude and fiber size, which determine the size of the VoI and hence the number of fibers that can be captured in the VoI as shown in (3).

Finally, we combined the probabilities for activating different fiber sizes to determine the probability of recruiting a particular number of fibers at specific current amplitudes. To obtain this total probability, we needed to account for all possible combinations of fiber recruitment that yielded the specified total number of fibers (N_{rec}) as in

$$\boldsymbol{P(N_{rec}|I,\{(fD_1,x_1),(fD_2,x_2),\ldots,(fD_n,x_n)\}) = \sum_i \prod_j P\left(C_{i,j}|I,\{fD_j\}\right).} \quad (9)$$

where each x_j is an upper bound on the number of fibers of diameter fD_j in which we are interested, with $x_j \leq N_{rec}$ and $\sum_{j=1}^{n} x_j \geq N_{rec}$. The matrix $\boldsymbol{C}$ has rows indexed by i and n columns indexed by j. Each column corresponds to a particular fiber diameter. Each row i, with $\sum_{j=1}^{n} C_{i,j} = N_{rec}$ and $C_{i,j} \leq x_j$, represents one of the possible combinations of fiber recruitment across fibers sizes. The fiber diameters $\{fD_1,\ldots,fD_n\}$ can be any subset of the fiber diameters listed in Table 4.1 or Table 4.2. The maximum possible value of N_{rec} is equal to the sum of N_{VoI} values for the fiber diameters in the set $\{fD\}$; that is, one cannot recruit more fibers than could be packed into the VoI. Using (9) we were able to estimate the probability of recruiting specific

combinations of fibers (e.g. one medium fiber and one large fiber or two medium fibers and one large fiber) (see appendix A for further details).

4.2.3 Electrophysiology

Data reported from a previous in vivo study were used for comparison with model predictions. For details on the methods used to collect these data refer to [74]. The University of Pittsburgh Institutional Animal Care and Use Committee approved all procedures. To summarize, adult cats were implanted with penetrating microelectrode arrays in the L7 DRG for stimulation and a 5-pole nerve cuff electrode around the sciatic nerve for recording elicited antidromic action potentials. Single channel microstimulation in the DRG was performed to determine the threshold stimulus amplitude at which a response could be recorded in the nerve cuff using stimulus-triggered averaging. A charge-balanced biphasic, cathodic-leading 200 μs pulse followed by a 400 μs anodic pulse was used for stimulation. Thresholds were typically between 1 and 3 μA and approximately 97% of the fibers were recruited at amplitudes less than or equal to 6 μA [74]. We therefore chose this value as an upper limit on stimulus amplitude for these simulations.

The nerve cuff had two recording sites at a fixed separation distance (8 mm). The propagation delay was measured within the nerve cuff as the time it took for an action potential to propagate between the two recording sites. The electrode separation distance divided by this propagation delay yielded the conduction velocity for an activated unit. An estimate of the fiber diameter was obtained by dividing the conduction velocity by 5.66 based on [76]. Fiber

diameters found in the in vivo study ranged from 7.3 - 16 μm, which drove the selection of the fiber sizes tested in our model.

4.3 RESULTS

In this study, we examined the current-distance relation using the single-fiber model. Next, we compared the probabilities of recruiting fibers of various diameters (7.3 - 16 μm). Finally, we used the population model to predict recruitment in a heterogeneous population of fibers in the DRG. Simulations were run to determine the number of fibers, by size, that would be activated in response to a given stimulus intensity. We verified these results against DRG microstimulation recruitment data reported previously [74].

4.3.1 Current-distance relationship

Activation of a neural fiber depends on several factors, including stimulus waveform and amplitude, fiber size, and distance from the stimulating electrode. For example, the inverse relationship between the extracellular voltage and the distance between the electrode and a node of Ranvier drives the nonlinear behavior of the current-distance relation as expressed in (1). Figure 4.3A illustrates the effect of increasing fiber diameter on the current-distance relation, as predicted by the single-fiber model. In general, the electrode-to-node distance increases with the stimulus amplitude. At higher intensities, the larger diameter fibers can be activated at much greater distances. This gives rise to the so-called ‘reverse recruitment’ phenomena that has been described for muscle activation with epineural electrodes [59, 77]. However, for amplitudes

below 10 μA (see inset in Figure 4.3A), there is little difference in the current-distance relationship for fibers of different diameters. Thus, at these low intensities, the radius of the VoI is effectively the same for all myelinated fibers within the range tested. Although the VoI is the same for these fibers, this does not mean that these different sized fibers have equal likelihood of being recruited in the 0-10 μA range. In order for a fiber to become activated, one of its nodes of Ranvier must be captured within the VoI.

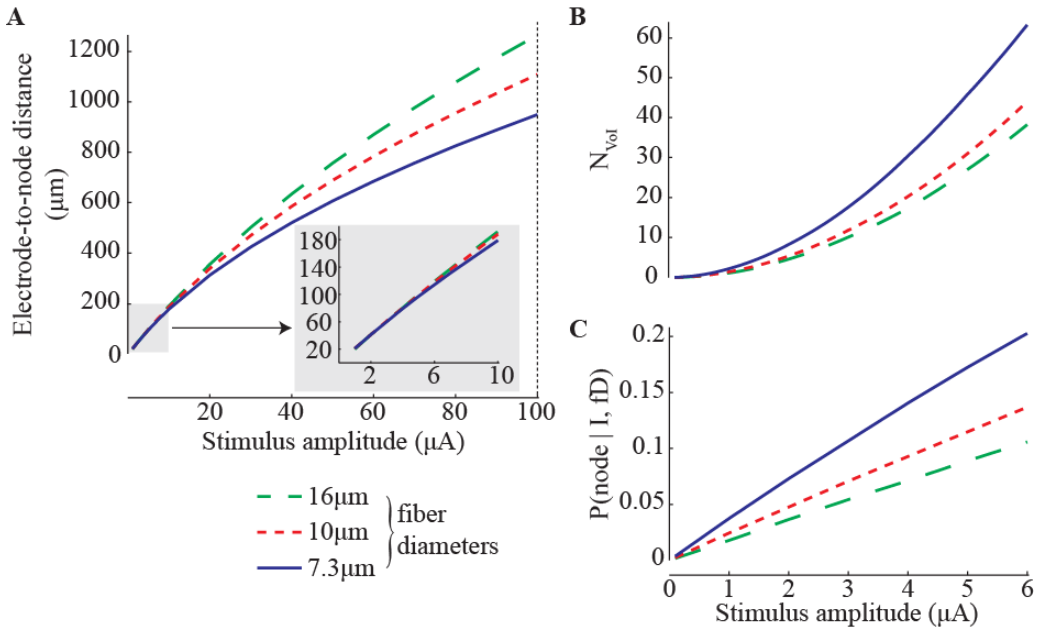

Figure 4.3 Effects of fiber diameter on current-distance relation, fiber packing and probability of having a node in the VoI. (A) Current-distance relationships from single-fiber model. Electrode-to-node distance corresponds to the radius of a spherical VoI centered about a stimulating electrode. (B) The number of fibers that can be packed into the VoI assuming a packing ratio equal to 1. (C) Probability of capturing a node of Ranvier in the VoI as predicted by (7). Fiber sizes of 7.3 μm, 10 μm and 16 μm were simulated.

To compare the likelihood of recruiting different fiber sizes, we simulated populations of neurons assuming a packing ratio (R_{DRG}) of 1 in (3) to estimate the number of fibers passing through the VoI. Figure 4.3B shows the number of fibers penetrating the VoI, which increases in size with the stimulation intensity (1-6 μA). Note that there are considerably more 7.3 μm diameter fibers penetrating the VoI. This is because there are nearly twice as many 7.3 μm

diameter fibers as there are 10 and 16+ μm fibers in the DRG (see Table 4.1). In addition, there is a higher probability of capturing a node within the VoI (see Figure 4.3C) for the 7.3 μm diameter fibers because the internodal length (L_{int}) is shorter (Table 4.1), as shown in (7). Thus, Figure 4.3B and Figure 4.3C suggest a bias towards recruitment of smaller diameter fibers, due to the relatively greater number of 7.3 μm fibers and the higher number of nodes per unit length as compared to the larger fibers.

4.3.2 Thresholds for single-fiber recruitment in a population

Using the population model, we first explored the effects of the packing ratio on recruitment predictions based on (9). We ran simulations to predict the probability of recruiting at least one fiber, varying the stimulus intensity from 1-6 μA and the packing ratio from 0.1 to 1.0 in (3). The model predictions are shown in Figure 4.4. In general, the probability of recruiting at least one fiber is very low for stimulation amplitudes < 1 μA and increases with the stimulus amplitude. Note that the rate of increase is much faster when the packing ratio is high. We defined the recruitment 'threshold' as the stimulation amplitude that yields a 0.5 probability of recruiting at least one fiber, indicated by the dotted line in Figure 4.4. The recruitment threshold is ~1 μA when the packing ratio is 1, but increases to nearly 3 μA when the packing ratio is only 0.1. The series of '+' symbols indicate the cumulative probability of recruitment from subject 1 in our previous in vivo experiment [74]. We found that for a packing ratio of 0.26, the population model provided an excellent fit ($R^2 > 0.9$) to those in vivo data. We also used the population model to fit recruitment data for subject 4 from the same published data and found a packing ratio of 0.11 yielded the best fit ($R^2 > 0.9$). The variability in the packing ratios for these two

experiments is likely due to differences in the electrode placement between the two experiments; the density of fibers around the electrodes was apparently higher in subject 1 than in subject 4 as suggested by the higher packing ratio found for subject 1. Using the model to fit the electrophysiology data across all four subjects, the best packing ratio was found to be 0.2 (R^2 > 0.9). Thus, despite the potential for large differences in fiber density throughout the DRG, the range of values for the packing ratio is fairly narrow (R_{DRG} = ~0.1 - 0.3) for the data obtained in our in vivo study.

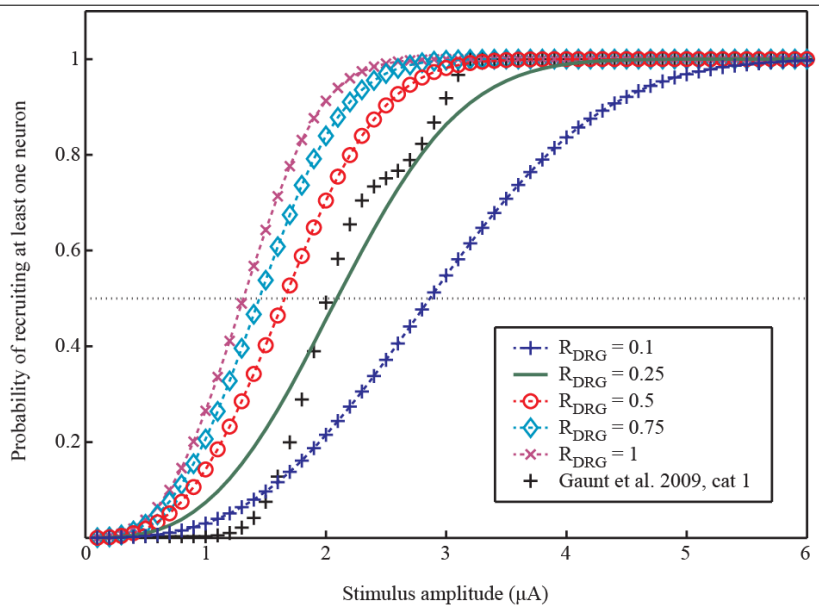

Figure 4.4 Sensitivity of population model to the packing ratio. The black markers represent published electrophysiology data for a single subject (Gaunt, Hokanson et al. 2009). The other traces represent model simulation results of recruiting at least one fiber for different packing ratios. The model best predicts the electrophysiology data for a packing ratio of approximately 0.26 (R^2>0.9) for cat 1, and 0.2 (R^2>0.9) across subjects.

Gaunt and colleagues also observed that in 53% of electrodes tested on four animals, medium diameter fibers were recruited at lower current amplitudes than the larger fibers recruited with the same stimulating electrode [74]. This result suggests a small bias favoring recruitment of medium-diameter fibers when stimulating at the lowest intensity that yielded an identifiable response (i.e. a so-called threshold response). Gaussian distributions were fit to these

data using the mean and standard deviation computed for the two sets of fiber sizes $\{fD\}_{medium}$ and $\{fD\}_{large}$. The distributions were normalized such that their integrals were equal to the number of observations for each fiber size category and divided by the total number of observations (n=10/24 and 14/24 for recruitment of large and medium fibers at threshold, respectively). The solid traces in Figure 4.5 illustrate the probabilities, given that a fiber was recruited at threshold, of observing a large or medium size fiber in the in vivo data. For both fiber size categories, the range of stimulus amplitudes accounting for threshold was similar. These data demonstrate a slightly higher probability of recruiting medium-diameter fibers. Next, we investigated model predictions for comparison to these in vivo results.

We examined this bias with the population model by calculating the probability of recruiting only one large (12.8 – 16+ μm) or one medium (7.3 – 11.5 μm) diameter fiber in isolation (setting x_j = 0 in (9) for the other group of fibers) across a range of stimulation amplitudes. The recruitment of exactly one fiber in isolation corresponds to the threshold responses that were recorded in the previous in vivo study. For this analysis, we used a packing ratio of 0.26 to allow direct comparison of the model result to the data set for subject 1 in the in vivo study (see Figure 4.4). The population model was used to determine the probability of recruiting exactly one large fiber and no medium fibers or exactly one medium fiber and no large fibers. The probability distributions for recruiting one large or one medium fiber both have a maximum at 2.3 μA, and the means and ranges of these distributions matched well with the distributions of threshold currents found in vivo. However, across the range of current amplitudes tested, the probability of recruiting one medium fiber is more than twice that of recruiting one large fiber (Figure 4.5). Thus, the population model suggests a much stronger bias favoring recruitment of medium fibers than was observed in vivo (see discussion).

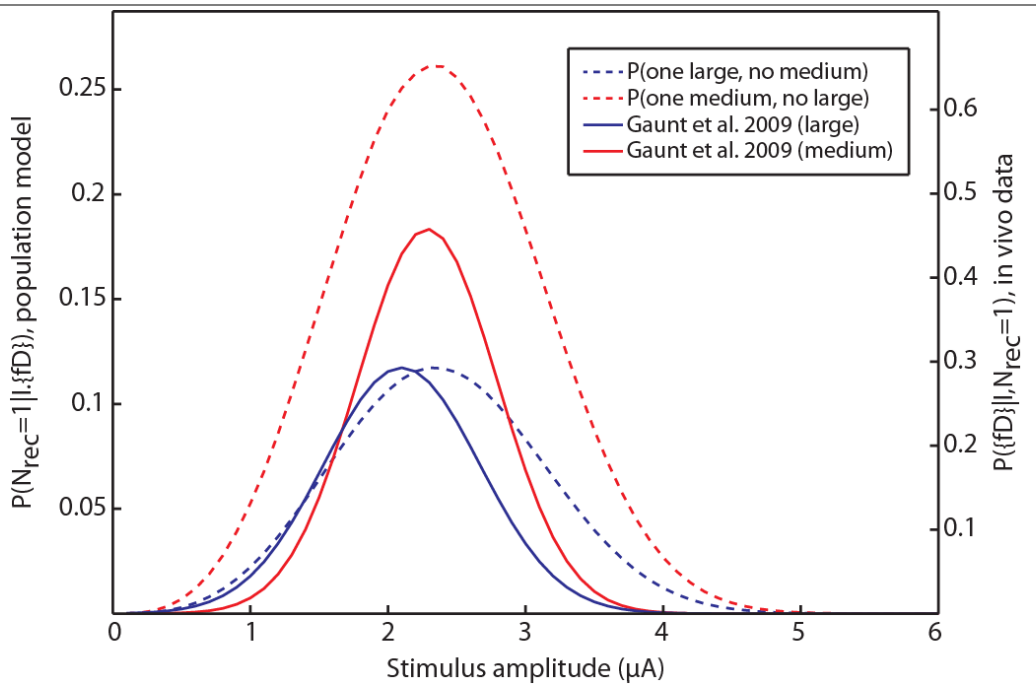

Figure 4.5 Comparison of model predictions to electrophysiology data at threshold amplitudes. The solid traces represent the probabilities of recruiting a fiber from one of the two fiber sets $\{fD\}_{medium}$ and $\{fD\}_{large}$, given that a fiber was recruited, as a function of stimulus intensity. The dashed traces represent model predictions for recruiting a fiber from one of the two sets as a function of stimulus intensity. The gray traces represent the probabilities of recruiting exactly one large fiber (12.7-16+ μm). The black traces represent the probabilities of recruiting exactly one medium fiber (7.3-11.5 μm). The y-axis for the model data is on the left and the y-axis for the electrophysiology data is on the right (Gaunt, Hokanson et al. 2009).

4.3.3 Fiber recruitment to evoke EMG response

In chapter 2, we presented analyses of EMG as evidence of muscle activation in response to electrical stimulation of VR or DRG. We found that the median stimulus threshold to observe muscle activity in response to VR stimulation was lower than that for DRG stimulation, at 12 and 25 μA, respectively. Using the computational model, we estimated the numbers of alpha motor neurons recruited as a function of VR stimulation. First, we entered tissue parameters into the population model, such that it represented feline L7 VR (Table 4.2). Using the same method to determine DRG packing ratio, we chose 0.1 to represent the average VR packing ratio (see

discussion), and tested stimulus intensities of up to 8 μA. For comparison, we performed simulations for recruitment of sensory afferents in the DRG, assuming a packing ratio of 0.2 (see discussion).

Table 4.2 Model parameters for feline L7 VR. For each fiber diameter included in the model, the table lists the number of fibers (N_{fD}) found in the feline L7 VR based on (Risling, Aldskogius et al. 1983), as well as the fractional area of the fibers of interest occupied by each fiber size (R_{fD}), and the intermodal lengths (L_{int}) based on (Nilsson and Berthold 1988).

fD (μm)	5.7	7.3	8.7	10	11.5	12.8	14+
N_{fD}	125	530	840	760	510	55	55
R_{fD}	0.04	0.18	0.29	0.26	0.18	0.02	0.02
L_{int} (μm)	500	750	1000	1150	1250	1350	1400

For each stimulus amplitude, the number of fibers that produced the highest probability of recruitment, $P(N_{Rec}|I)$, was taken as the number of fibers recruited at that intensity. Figure 4.6 shows the relationships between stimulus amplitude and the number of fibers most likely recruited, for VR and DRG stimulation. These data were fit to functions of the form $N_{rec} = A(I-I_0)^2$, where I_0 = 2 μA and A = 0.45 and 0.30 fibers/μA^2 for VR and DRG stimulation, respectively ($R^2 > 0.99$). We were particularly interested in the number of alpha motor neurons recruited at the threshold to elicit EMG activity in response to VR stimulation, as well as the number of afferents recruited at threshold in response to DRG stimulation. We estimated that VR stimulation at 12 μA activates approximately 45 motor neurons. We expected the number of alpha motor neurons activated at threshold to be much closer to one. O'Donovan and colleagues noted lower thresholds for VR stimulation of 5 – 10 μA [32]. The model estimates that approximately 4 alpha motor neurons are recruited at this level in response to VR stimulation. Likewise, DRG stimulation at 25 μA activates approximately 160 motor afferents. However,

limitations in the computational model and the electrophysiology instrumentation likely caused overestimations of both the thresholds and the numbers of fibers recruited.

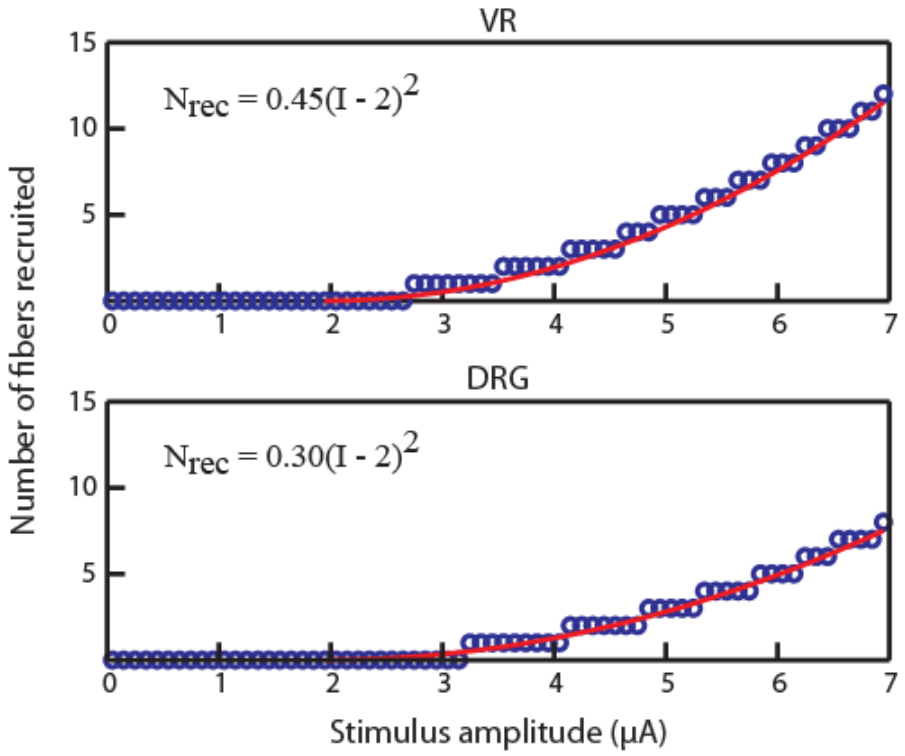

Figure 4.6 Recruitment of multiple fibers in a heterogeneous population across stimulation amplitudes in VR (top) and DRG (bottom). Blue circles denote model predictions and red traces denote fits of a power function to the model predictions. N_{rec} represents the number of fibers recruited as a function of stimulus intensity I.

4.4 DISCUSSION

To address the second specific aim, we developed this computational model, which we used to answer questions about the number and sizes of primary afferent fibers recruited by stimulation in the VR or DRG. Previously published computational models were designed to address recruitment in specific peripheral nerve structures using a deterministic approach. Here we specified the stimulus intensity and fiber sizes of interest to define a volume of tissue activated.

The model used a probabilistic approach to estimate recruitment of fibers in the VR or DRG, but it can be adapted readily to model different tissue morphologies given information on the distribution of fiber sizes in the tissue. Finally, we compared model predictions to data collected from in vivo experiments and explored the factors accounting for the pattern of recruitment observed.

4.4.1 Recruitment order

We began by running simulations to explore the recruitment of fibers based on size, which suggested that smaller fibers were as likely as or more likely to be recruited than larger fibers over the range of fiber sizes and stimulus intensities tested. At large stimulus intensities (i.e., $I >$ ~30 μA), the electrode can activate larger fibers at a greater distance compared to smaller fibers, as demonstrated by the current-distance relationship [78]. However, at the stimulus intensities that we tested (less than 10 μA) the current-distance relationship was effectively the same for the different fiber diameters (Figure 4.3A).

The difference in probabilities of recruiting different-sized fibers was due to a combination of two main factors: 1) the number of fibers of a given size that are likely to be present in the VoI and 2) the likelihood of a fiber having a node of Ranvier in that VoI. Equation (3) and Figure 4.3B showed that as fiber diameter decreased, the number of fibers that were likely to be packed into a VoI increased. This behavior was influenced by the distribution of fibers by size (N_{fD}). In the case of feline L7 DRG, the distribution of fiber sizes is skewed toward medium size fibers over larger fibers. Equation (7) and Figure 4.3C showed that as fiber size decreased, and accordingly as internodal length decreased, the probability of those fibers having

a node of Ranvier in the VoI increased. Because of these two factors, there was a greater likelihood of recruiting a smaller fiber before a larger fiber in our model.

4.4.2 Recruitment in a population

After examining recruitment order, we explored the contribution of the packing ratio to recruitment in a population. The impact of the packing ratio on predictions of recruitment with the population model is important because of the direct physiological implication of this parameter. We found that the model best fit the recruitment data observed in vivo for a packing ratio of 0.2 ($R^2 > 0.9$). To validate this parameter, we used (4) to calculate a value for the packing ratio based on measurements of A_{DRG}, which are approximately 4.9 – 7.1 mm^2 for DRG diameters measured to be 2.5 – 3 mm. Using the fiber diameter distribution data from Risling and colleagues [68], the area occupied by fibers larger than or equal to 7.3 μm is approximately 1.15 mm^2; this is the value of the numerator in (4). Dividing this area by the cross-sectional area of feline DRG yields a packing ratio of 0.16 – 0.23. This packing ratio range corresponds closely to the range found in our simulations (0.11 – 0.26). Furthermore, using the 'best-fit' values for packing ratio and solving (4) for A_{DRG} yields DRG diameters in the range 2.4 – 3.6 mm, which again agrees well with our measured values. In similar fashion, using fiber diameter distribution data for feline L7 VR from Risling and colleagues [68], the packing ratio for a 1.5 mm diameter VR would be 0.12. While one might assume that the VR would be much more densely packed, perhaps due to its lack of cell bodies and smaller tissue size, the packing ratio is quite similar to that of the feline L7 DRG. This average packing ratio may differ in other spinal roots, dorsal and ventral.

The DRG packing ratio was varied to evaluate the sensitivity of the model to this parameter. As the packing ratio increased, the likelihood of recruiting neurons at lower amplitudes increased because of the greater number of fibers passing through the VoI (Figure 4.4). DRG are heterogeneous structures and the packing ratio represents only an average value; the packing ratio may be higher or lower in different sections of the tissue (Figure 4.1B). For example, the local volume around a stimulating electrode may have a high packing ratio if the electrode is surrounded by a bundle of fibers, or it may have a small packing ratio if there are cell bodies occupying a large portion of the VoI.

To explore the recruitment of different fiber sizes, we simulated a heterogeneous population of neurons, varying the fiber sizes included in the population. Figure 4.5 demonstrates the different contributions of medium fibers (7.3 μm - 11.5 μm) versus large fibers (12.8 μm – 16+ μm) to the probability of recruiting a fiber in this population. This figure shows that when stimulating at low intensities, the chance of recruiting a single medium fiber is more than twice that of recruiting a single large fiber. Thus, the population model suggests a much stronger bias favoring recruitment of medium fibers than was observed in vivo. One likely source of this discrepancy stems from the differences in the ability to record propagating action potentials from large and medium fibers in a nerve cuff, as was used in our in vivo study. The recorded voltage of an extracellular signal increases in a power law fashion with increasing conduction velocity, which is closely related to fiber size [79]. Thus, action potentials from smaller fibers are more difficult to detect and it is possible that some active medium fibers may have gone undetected in the nerve cuff recordings used to identify thresholds in the in vivo study.

4.4.3 Recruitment in response to VR or DRG stimulation

Finally, we examined recruitment of fibers in response to stimulation at the threshold to elicit EMG activity. For this analysis, we introduce VR stimulation for comparison to DRG stimulation. Under ideal circumstances, we would expect activation of a single alpha motor neuron to result in detectable EMG activity. However, the model estimated a large number of alpha motor neurons recruited in response to stimuli at 16 μA – the mean threshold at which activity was recorded in the EMG. First, the model makes simplifying assumptions about conductance through the extracellular medium, which were not validated at these higher amplitude levels. If the model underestimates the resistivity of the medium as a function of distance from the electrode, it will in turn overestimate recruitment of fibers in response to a given stimulus. In addition, the thresholds that we reported are larger than those reported by O'Donovan and colleagues for VR stimulation [32]. If we use the model to estimate fiber recruitment at the thresholds that these investigators published, that estimate is more reasonable. For these reasons, the model estimates of fiber recruitment in response to DRG stimulation at the threshold to record EMG activity were also likely overestimated.

Modeling the VR can offer insights into the number of fibers required to generate force, although we are limited in our ability to predict fiber recruitment at stimulus amplitudes much higher than threshold (see Assumptions and limitations subsection). One might even relate the VR packing ratio and the rate of current spread to the steepness of the force recruitment curve. However, the model does not simulate all steps in the reflex pathways between fiber recruitment in response to DRG stimulation and forces generated. To explore motor responses evoked via DRG stimulation, we can use the model to predict the numbers and sizes of afferents recruited, then categorize these fibers into different modalities based on the likelihood of a fiber size

belonging to a particular sensory category (e.g. Ia muscle, II cutaneous, etc.). With estimates on the numbers and modalities of fibers recruited, we would also need to know not only the different types of reflex pathways, but also the number of afferents required to trans-synaptically activate motor neurons. For a hypothetical example, if a DRG channel has a threshold to elicit an EMG response of 10 μA, then the model would predict that approximately 20 fibers of at least 7 μm were recruited. This would mean roughly 20 afferents were activated to trans-synaptically activate a motor neuron. In addition, if 20 μA were required to produce 0.1N of force, then the DRG model would suggest that roughly 100 fibers were necessary to evoke that response.

4.4.4 Assumptions and limitations

In this chapter, we assumed that the extracellular medium was infinite, homogeneous and isotropic [31]. Ranck and Bement showed that the extracellular medium of the spinal cord dorsal columns in cat is anisotropic, with a longitudinal resistivity of approximately 300 Ω-cm and a transverse resistivity of approximately 1200 Ω-cm [73]. This anisotropy would change the shape of the VoI from spherical to ellipsoidal by altering the resistivity parameter (ρ_{ext}) to have a longitudinal and a transverse component, rather than being direction-insensitive. We altered the model to assume an ellipsoidal VoI with these extracellular resistivity parameters and found no significant difference in the probability of recruiting one or a few fibers (data not shown). Therefore, for the simulation conditions that we tested and presented in this chapter, we felt that this simplifying assumption of using a spherical VoI was justified.

We did not include cell bodies in the model, assuming that the site of activation would always occur at the nodes of Ranvier rather than at the soma. Amir and Devor [80] developed a

model for frog DRG neurons to explore the soma's role in propagating an action potential. We used their model to test the DRG neuron's response to extracellular stimulation as a function of current amplitude and electrode placement (data not shown). We found that, regardless of current amplitude or electrode position, we could not activate the neuron by stimulating the cell body. In addition, previous work has shown that the site of action potential generation is always at a node of Ranvier and not the cell body [29, 81, 82]. This work led us to assume that only nodes of Ranvier were potential sites for activation in response to extracellular stimulation within the ranges of stimulus parameters tested.

Only stimulus amplitudes less than 100 μA were tested with the single-fiber model and less than 10 μA were tested for the population model. The larger amplitude range (0 – 100 μA) was tested with the single-fiber model to explore the current-distance relationship over a wide range of currents. The smaller current range, less than 10 μA, was of particular interest here because intraneural microstimulation experiments have demonstrated that this lower current range is sufficient to elicit neuronal responses [36, 74]. In addition, stimulation currents less than 6 μA accounted for 97% of the threshold responses reported for in vivo experiments [74]. Of equal relevance, the single-fiber model predicts that as the current intensity is increased above 10 μA, the distance an electrode can be from the fiber to achieve recruitment increases beyond 200 μm (Figure 4.3A). Commercially available electrode arrays have inter-electrode spacing ranging from 200-400 μm [5, 74]. This spacing appears to be appropriate based on the model's results for recruiting small numbers of neurons at stimulus amplitudes below 10 μA, though different recruitment circumstances may require that this spacing be altered.

Finally, we only included fiber sizes for which we had validated single fiber models. These single fiber models included sizes of 5.7, 7.3, 8.7, 10, 11.5, 12.8, 14, 15, and 16 μm (Table

4.1 and Table 4.2). These fiber sizes correspond to α-motor neurons in the VR or large cutaneous and muscle afferents in the DRG. The model ignores smaller fibers, such as γ-motor neurons in the VR or Aδ and C fibers in the DRG. Since we are mostly interested in recruitment of α-motor neurons in response to VR stimulation, this limitation may be acceptable. However, we cannot predict the likelihood that DRG stimulation might cause pain through activation of C fibers. In addition, we are unable to explore reflex pathways that take advantage of Aδ fibers, such as withdrawal reflexes to noxious stimuli. If these smaller sizes were included, we could estimate the number of these fibers recruited and, knowing roughly how many are required to activated motor neurons through reflex pathways, predict the motor responses.

4.5 CONCLUSIONS

We have developed a model that predicts recruitment of sensory fibers in the DRG in response to extracellular microstimulation. The model offers some insights into the factors governing recruitment in a mixed population of fibers. Our results indicate that at low intensities (< 10 μA), smaller fibers are more likely to be recruited as compared to larger fibers over the ranges of fiber sizes and distributions considered here. Furthermore, the results from these simulations suggest that previous in vivo studies may have underestimated the chance of recruiting medium diameter fibers with primary afferent microstimulation in the DRG. The model was also able to simulate the recruitment of multiple fibers, which can be used to predict, for a given stimulus condition, the most likely number of fibers, by size, that will be recruited.

The model has a number of potential applications. This model could be used to aid the design of microelectrode arrays, taking advantage of the model's ability to predict the number

and size of axons recruited as a function of stimulus intensity. The model is able to provide information on the size of the VoI and thus the geometry of an array could be designed to minimize overlap between adjacent VoIs while maximizing specificity for target fibers. Besides stimulus intensity, other stimulus parameters may be tested, such as pulsewidth or polarity, on the effects of recruiting neurons in a population. In addition, other fiber sizes (less than 7.3 μm) may be incorporated into the model to represent other sensory modalities, such as nociceptors, thermal receptors, or other primary afferent fibers. For example, it is currently difficult to ascertain the degree to which we are recruiting pain fibers in these primary afferent microstimulation paradigms. Given the distribution of nociceptive fibers, the population model could offer some insight into the probability of activating these other fiber types.

5.0 SUMMARY AND CONCLUSIONS

Having presented results, which addressed the specific aims of this dissertation, we provide here context with which to consider those results. The impact on the field is discussed, examining not only the engineering contributions made, but also the contributions to neuroscience. Finally we propose several extensions on this work, utilizing multiple methods, including electrophysiology, computational modeling, and histology, as had been done in approaching the problem initially. We conclude that further exploration of VR and DRG stimulation is worthwhile.

5.1 SUMMARY OF RESULTS

In addressing the first specific aim, we categorized the functional responses to VR or DRG stimulation with electrophysiology experiments in rats and cats. We used several metrics to evaluate the performance of these two potential interfaces, including stimulus threshold, selectivity, force recruitment slope, and force magnitude. VR stimulation produced EMG responses at significantly lower thresholds than DRG stimulation, but we considered both threshold ranges low compared to other interfaces, such as nerve cuffs. We noted that our thresholds were somewhat higher than what has been observed in the literature, but this difference was likely due to limitations in our EMG recording setup. Both VR and DRG interfaces demonstrated selectivity for target muscles, where the difference between thresholds to

activate antagonist muscle groups was 2 – 20 μA. This range of threshold difference is not trivial given the low thresholds observed for both interfaces. VR and DRG stimulation produced force recruitment curves with small slopes, suggesting more controlled, graded force recruitment. However, both interfaces demonstrated approximately linear increases in force in response to increased stimulus amplitude, up to the limit of the stimulator. Force vectors were consistent for both interfaces as well, with single-channel DRG stimulation capable of producing sufficient force to bear a significant percent of body weight for use in standing or walking. VR stimulation produced nearly as much force. These interfaces performed as well as ISMS and IFMS on most metrics. We defined selectivity differently than has been done for other interfaces, making direct comparisons difficult for this metric.

To address the second specific aim, characterizing the pattern of fiber recruitment, we developed a computational model to estimate the number and sizes of fibers recruited in response to VR or DRG stimulation. We validated the model using published data from an in vivo experiment and explored the pattern of fiber recruitment. We determined that there was a bias for recruiting smaller fibers before larger fibers in response to intraneural stimulation. The model also estimated higher thresholds to activate fibers in response to DRG stimulation versus VR stimulation, which was consistent with our electrophysiology results. This second specific aim extended our exploration in the another metric of performance: recruitment order. Interfaces such as the nerve cuff recruit large fibers before small fibers, but IFMS appears to recruit whichever fiber has the closest node of Ranvier to the electrode. This improved access to fibers of different sizes has the potential to improve selectivity and incorporate strategies such as interleaved stimulation for improved fatigue-resistance.

This model gives us insight into the mechanisms by which we evoke motor responses to intraneural stimulation by providing some intuition for the size and numbers of fibers recruited. We note that the model does not account for the trans-synaptic activation of motor neurons following activation of afferent fibers in the DRG. Further understanding of the mechanisms involved in stimulating afferents to produce reflexive motor responses is necessary when interpreting results from computational and electrophysiological experiments. The model also does not include validated single-fiber models for fiber sizes less than 5 μm, which would include gamma motor neurons in the VR or pain fibers in the DRG. Further investigations in fiber recruitment could use this model because of its generalizability for different peripheral tissue structures, assuming a bundle of axons. It can also inform the design of interfaces, giving insights to such parameters as electrode geometry and spacing.

5.2 IMPACT ON FIELD

The work presented in this document provides a fundamental understanding of intraneural VR or DRG stimulation for FES applications, in particular afferent stimulation for accessing reflex pathways. Afferent stimulation has previously been considered for restoring sensory feedback, but there is less precedent for afferent stimulation to produce motor responses for use in FES systems. This work supports the idea that afferent stimulation can be used to control systems that were lost to paralysis. For example, this approach could be applied to other systems, such as bladder control or respiratory control, taking advantage of reflex pathways.

In this work, we have also presented a computational model to examine recruitment of fibers in response to low intensity intraneural stimulation. Computational modeling has made

important contributions to our understanding of fiber recruitment in response to electrical stimulation. Previous models have simulated extraneural stimulation or used finite element models of a specific nervous tissue structure. These models were not suitable for addressing our questions of fiber recruitment in spinal roots following stimulation through a penetrating microelectrode. In addition to modeling intraneural stimulation, our model provides access to parameters that vary by nervous tissue, which allows us to adapt it to different tissue structures, such as VR or DRG. This tool provided important insights about the size and number of fibers recruited in response to spinal root stimulation, and therefore the mechanisms by which we generated motor responses.

The results from this preliminary work support an argument for VR and DRG stimulation as potential interface strategies. VR and DRG interfaces performed similarly on a number of metrics, on par with IFMS and ISMS. Indeed, there remain the potential benefits of VR or DRG stimulation to provide a physical interface that is more mechanically stable than IFMS and to provide a central access point to all the fibers innervating target muscles. Therefore, we can discount neither of them at this point. Further work is needed to explore their potential for FES applications.

5.3 FUTURE DIRECTIONS

A number of methods are necessary to advance our understanding and performance with VR and DRG stimulation, including electrophysiology, computational modeling, and histology. We identified some limitations in the electrophysiology work presented here. For example, we could use improved EMG electrode designs to achieve more sensitive muscle activation measurements.

Higher resolution variation of the stimulus frequency parameter would allow us to explore its effects more carefully. We were unable to produce maximal muscle contractions because we did not have complete access to all the neurons innervating a muscle. A sciatic nerve cuff would give us this access and evoke maximal muscle contractions of TA and MG muscles, which we can use to normalize our EMG data. In addition, measuring muscle contractile forces from these muscles individually, rather than endpoint force, would give us more information and allow us to compare our results to published work for other interface designs, such as IFMS. We would design this muscle contractile force measurement to prevent our previous endpoint force measurement limitations imposed by the force transducer that we used. Furthermore, kinematic data could give us information about the functional responses beyond what we can observe through fixed endpoint force measurements. Future electrophysiology experiments might benefit by focusing on the ankle actuators, fully exploring the stimulus parameter space.

The computational model included fiber sizes of at least 5 μm in diameter. While this range may be sufficient to examine recruitment of fibers related to motor function, it would be useful to validate smaller fiber sizes that represent Aδ and C fibers, which encode such sensory perceptions as temperature and pain. This addition to the model would allow us to estimate the likelihood of recruiting pain fibers in response to DRG stimulation, for example. In addition, the simplifying assumptions for the extracellular medium limited the model's ability to estimate fiber recruitment at current amplitudes above 5 μA. A more accurate description of the electric field through which the stimulus current travels would be a significant improvement.

Histological methods can be employed to address a number of questions. Future work should address the subjects' immune responses to chronically implanted penetrating electrodes. This problem remains one of the impediments to development of this technology. In addition, we

designed a tracer study to label neurons innervating a pair of antagonist muscles, TA and MG (see appendix B). We can address two important questions with this study: (1) Are fibers innervating distinct muscles, especially antagonists, clustered distinctly? and (2) Are activation patterns observed from electrophysiology studies predominantly a function of the distribution in the tissue of fibers by target of innervation? The first question helps us evaluate the potential for these interfaces in that distinct clustering would improve selectivity for target muscles, whereas uniform distribution of fibers, without distinct clustering, would result in very poor selectivity. Given the electrophysiology results presented here, we can hypothesize that there will be some degree of distinct clustering of fibers by target of innervation. The second question, regarding activation patterns, offers us an insight into the mechanisms by which we activate the muscles as observed and may give us an expectation to inform further experimentation.

Some of the groundwork has been laid for evaluating VR or DRG stimulation to restore motor function following paralysis. Acutely, VR and DRG stimulation performed in similar fashion to other interfaces, such as IFMS and ISMS, and they maintain some of their advantages, such as mechanical stability and central access to fibers innervating target muscles. Further exploration of these interfaces is warranted both to judge their performance and to compare them to other interfaces.

APPENDIX A

DERIVATION FOR EQUATIONS FOR COMPUTATIONAL MODEL

This appendix provides additional information on the derivation of equations used to estimate the probability of capturing a node in the VTA. Additionally, we provide an example to illustrate how we estimated the probability of recruiting a given number of fibers from a set of fiber sizes as a function of stimulus amplitude.

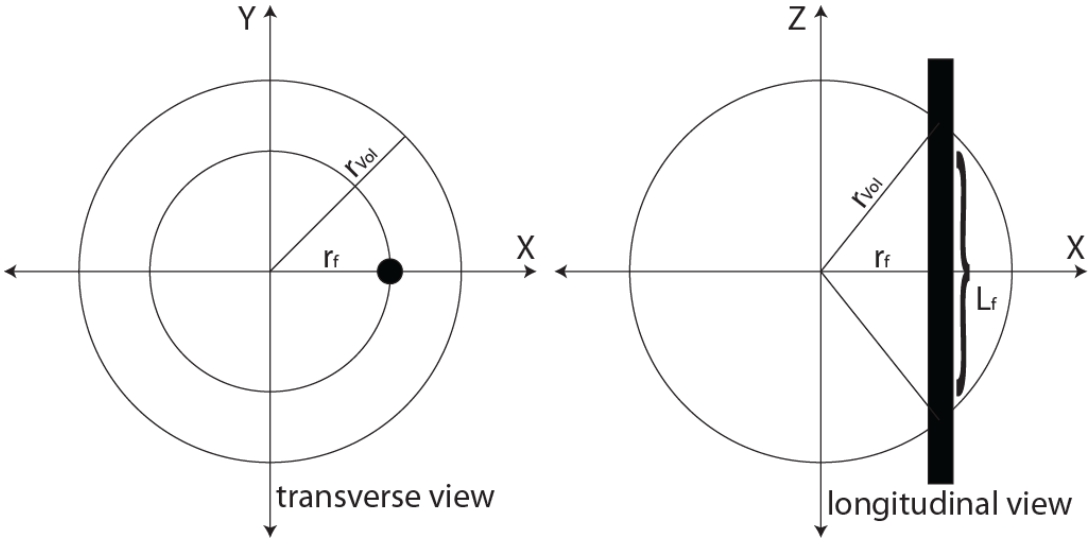

Figure A.1: Schematic depiction of fiber passing through spherical volume of tissue activated (VoI). The outer circle represents the boundary of the VoI, while the filled circle (transverse view) and the thick line (longitudinal view) represent the fiber of passage. The probability of a fiber having a node of Ranvier in the VoI is the ratio of the length of fiber contained within the VoI (L_f) to the internodal length of the fiber (L_{int}). This probability must be calculated for all possible locations of the fiber in the VoI to get a total average probability.

To describe the probability of a fiber of a given size having a node of Ranvier in the spherical VoI at a certain radial distance from its center, $P(node|I,fD,r_f)$, we divided the length of fiber encapsulated within the VoI (L_f) by the internodal length of the fiber (L_{int}) as in

$$P(node|I,fD,r_f) = \frac{L_f}{L_{int}} \tag{A.1}$$

We expanded on the definition of L_f

$$L_f = 2\sqrt{r_{VoI}^2 - r_f^2} \tag{A.2}$$

using the Pythagorean Theorem with the radial position of the fiber in the transverse plane (r_f) and the radius of the spherical VoI (r_{VoI}) as the hypotenuse (see figure A.1). We then multiplied the probability of finding a node of Ranvier by the circumference of the circle with radius r_f, then integrated with respect to r_f over the range [0, r_{VoI}]

$$P(node|I,fD,\boldsymbol{L_{int}} > 2r_{VoI}) = \frac{\int_0^{r_{VoI}} L_f * 2\pi r_f \, dr_f}{L_{int} * \pi r_{VoI}^2} \tag{A.3}$$

to determine an average value of this probability. The integral was evaluated, using (A.2), to

$$P(node|I,fD,\boldsymbol{L_{int}} > 2r_{VoI}) = \frac{-\frac{4\pi}{3}[(r_{VoI}-r_f)(r_{VoI}+r_f)]^{3/2}\Big|_0^{r_{VoI}}}{L_{int} * \pi r_{VoI}^2} \tag{A.4}$$

and then simplified to

$$P(node|I,fD,\boldsymbol{L_{int}} > 2r_{VoI}) = \frac{4r_{VoI}}{3L_{int}} \tag{A.5}$$

However, if the diameter of the spherical VoI was larger than the internodal length of the fiber, then the probability of finding a node might exceed 1. We capped this probability at 1 by first setting (A.1) equal to 1 as in

$$P(node|I,fD,r_f) = \frac{2\sqrt{r_{VoI}^2 - r_f^2}}{L_{int}} = 1 \tag{A.6}$$

and then solving for r_f

$$r_f = \sqrt{r_{VoI}^2 - \left(\frac{L_{int}}{2}\right)^2} = r_{inL} \tag{A.7}$$

The radial position (r_f) at which the length of fiber encapsulated within the spherical VoI is equal to the internodal length is denoted as r_L. The integral from (A.3) was separated into two integrals to get

$$P(node|I,fD,\boldsymbol{L_{int}} \leq 2r_{VoI}) = \frac{\int_0^{r_{inL}} L_{int} * 2\pi r_f \, dr_f + \int_{r_{inL}}^{r_{VoI}} L_f * 2\pi r_f \, dr_f}{L_{int} * \pi r_{VoI}^2} \tag{A.8}$$

In the first integral, the length of fiber encapsulated within the sphere was set to the internodal length and the integral was taken over the range [0, r_L]. The second integral determined the average probability as in (A.3), but over the range [r_L, r_{VoI}]. Equation (A.8) was evaluated and then simplified to

$$P(node|I,fD,\boldsymbol{L_{int}} \leq 2r_{VoI}) = \frac{L_{int} * r_{inL}^2 + \frac{4}{3}[(r_{VoI} - r_{inL})(r_{VoI} + r_{inL})]^{\frac{3}{2}}}{L_{int} * r_{VoI}^2} \tag{A.9}$$

In the population model, (A.9) was used to describe the probability of a fiber having a node of Ranvier within the VoI in the case where the diameter of the VoI was larger than the internodal length of the specified fiber. Note that (A.3-5) are only valid for L_{int} greater than $2r_{VoI}$, whereas (A.8) and (A.9) are valid for L_{int} less than or equal to $2r_{VoI}$. In fact, (A.9) simplifies to (A.5) if r_L is set to zero; r_L approaches zero as the interval of r_f values over which the entire internodal length is captured by the VoI approaches zero.

Finally, using probabilities from (A.9), we estimated the probability of recruiting a given number of fibers from a set of fiber sizes as a function of stimulus amplitude (see 9). As an example, let us assume that there are three fiber sizes in a population, termed A, B and C. To determine the probability of recruiting two fibers among A and B, but no C fibers, we begin by finding that there are three ways to get two fibers: one A and one B; two A's and zero B's; zero A's and two B's. For each combination, the probabilities for each neuron's state are multiplied; these probabilities are then summed across combinations. The equation to get the probability of recruiting two fibers among A or B, without getting any C fibers is expressed as

$$P(2|I,\{(A,2),(B,2),(C,0)\}) = P(1|I,A)P(1|I,B)P(0|I,C) + P(2|I,A)P(0|I,B)P(0|I,C)\ldots$$

$$+ P(0|I,A)P(2|I,B)P(0|I,C). \qquad \text{(A.10)}$$

This example illustrates the general means by which we determined the probability of recruiting a given number of fibers from a group of specified fiber sizes, given the probabilities of recruiting various numbers of fibers for all fibers of interest at the specified current level.

APPENDIX B

PROTOCOL FOR ESTIMATING CLUSTERING OF FIBERS IN SPINAL ROOTS BY TARGET OF INNERVATION USING RETROGRADE TRACERS

This appendix outlines a protocol wherein retrograde tracers are used to track peripheral nerves from their distal targets of innervation to proximal locations in the VR, dorsal roots and DRG. This experiment would provide information on the amount of clustering of these neuronal fibers and thus a better understanding of the performance of an electrical interface in one of these locations.

B.1 INTRODUCTION

An effective neuronal interface for use in functional electrical stimulation must take advantage of the organization, such as it is, of the tissue structure in which it is implanted. ISMS targets somatotopically organized ventral laminae of the spinal cord. IFMS uses electrodes implanted in the peripheral nerve with fascicular organization. For these two interfaces, the target neurons are grouped together, such that the volume of tissue activated in response to microstimulation will recruit neurons innervating the same muscle group. Indeed, if there were little organization, or

clustering of neurons by target of innervation, then the interface would be inefficient, with many stimulating electrodes recruiting muscles and their antagonists simultaneously.

In this dissertation, we have proposed interfaces with the VR and DRG. Stimulation experiments showed that in roughly 50% of stimulus channels, in either VR or DRG, we were able to activate a muscle without activating its antagonist, which would have resulted in a co-contraction. While this evidence suggests some degree of organization, little is known about the clustering of fibers by target of innervation in the VR, dorsal roots or DRG. Here we present a method for injection retrograde tracers into distal peripheral nerves near their targets of innervation so that those neurons that supply a given muscle can be tracked to their positions in the spinal roots. This protocol is adapted from similar work done in sciatic nerve [83] and single-labeling work done in VR [84].

B.2 METHODS

This protocol begins by explaining the surgical procedure by which the retrograde tracers are injected into the peripheral nerves; this protocol focuses specifically on nerves supplying the co-contractors tibialis anterior and gastrocnemius. After the tissue is processed and imaged, spatial clustering analysis is performed to quantify the organization in the tissue structure.

In each adult rat ($n \geq 5$), weighing approximately 300-350 g, the posterior hindlimb was incised longitudinally from the popliteal fossa to mid-thigh and the biceps femoris was separated from the semitendinosus, thus exposing the sciatic nerve and its trifurcation. The tibial nerve, which innervates the gastrocnemius muscle, was cut and its proximal end dipped in a small well containing 5% FluoroGold (FluoroChrome, LLC, Denver, CO) for approximately 1 hour. The

area was then washed to remove excess tracer and prevent uptake of tracer into non-target tissues. Likewise, we cut the peroneal nerve, which innervates the tibialis anterior, and dipped it in a small well containing 2.5% Fast Blue (Polysciences, Inc., Warrington, PA) for approximately 1 hour and then washed the area. As an alternative to cutting these nerves, they can instead be crushed and injected with approximately 2 μL of their respective tracer dyes using a small-gauge Hamilton syringe. In addition, 5% True Blue (Invitrogen, Carlsbad, CA) can be used in place of Fast Blue. These fluorescent dyes were used to distinguish between the neurons innervating these two muscles; the emission wavelength for FluoroGold is 600 nm and that of Fast Blue and True Blue is 420 nm. This double-labeling technique allowed us to simultaneously view the distribution of neurons innervating the gastrocnemius and its antagonist tibialis anterior.

After closing the incision, the rat was given buprenorphine for pain twice per day post-operatively. After allowing three days for retrograde transport of the tracer dyes, the rat was perfused with 4% paraformaldehyde. The spinal roots were recovered from the rat and placed in 4% paraformaldehyde to post-fix the tissues, then 30% sucrose to cryoprotect them. These tissues were frozen and mounted for slicing on a cryostat into 10 μm transverse slices to view the cross sections of the neuronal fibers. Images of these slices were taken under fluorescence microscopy and analyzed. Cluster analysis as described by Prodanov and colleagues [84] was used to describe the degree of clustering of fibers for each of the two injected nerves as they course through the dorsal roots, VR and DRG. Additional analyses were performed to determine the degree to which clusters of fibers innervating the two co-contractor muscles overlapped in these tissues.

BIBLIOGRAPHY

1. NSCISC. *Spinal Cord Injury Facts and Figures at a Glance*. 2010 [cited; Available from: http://www.spinalcord.uab.edu.

2. AHA. *Heart Disease and Stroke Statistics*. 2010 [cited; Available from: http://www.americanheart.org.

3. CRF. *One Degree of Separation: Paralysis and Spinal Cord Injury in the United States*. 2009 [cited; Available from: http://www.christopherreeve.org.

4. Castro, M.J., et al., *Influence of complete spinal cord injury on skeletal muscle within 6 mo of injury.* J Appl Physiol, 1999. **86**(1): p. 350-8.

5. Mushahwar, V.K., et al., *New functional electrical stimulation approaches to standing and walking.* J Neural Eng, 2007. **4**(3): p. S181-97.

6. Green, D., *Prevention of thromboembolism after spinal cord injury.* Semin Thromb Hemost, 1991. **17**(4): p. 347-50.

7. Nash, M.S., B.M. Montalvo, and B. Applegate, *Lower extremity blood flow and responses to occlusion ischemia differ in exercise-trained and sedentary tetraplegic persons.* Arch Phys Med Rehabil, 1996. **77**(12): p. 1260-5.

8. Liberson, W.T., et al., *Functional electrotherapy: stimulation of the peroneal nerve synchronized with the swing phase of the gait of hemiplegic patients.* Arch Phys Med Rehabil, 1961. **42**: p. 101-5.

9. Moe, J.H. and H.W. Post, *Functional electrical stimulation for ambulation in hemiplegia.* J Lancet, 1962. **82**: p. 285-8.

10. Baldi, J.C., et al., *Muscle atrophy is prevented in patients with acute spinal cord injury using functional electrical stimulation.* Spinal Cord, 1998. **36**(7): p. 463-9.

11. Davis, J.A., Jr., et al., *Preliminary performance of a surgically implanted neuroprosthesis for standing and transfers--where do we stand?* J Rehabil Res Dev, 2001. **38**(6): p. 609-17.

12. Nash, M.S., et al., *Evaluation of a training program for persons with SCI paraplegia using the Parastep 1 ambulation system: part 5. Lower extremity blood flow and hyperemic responses to occlusion are augmented by ambulation training.* Arch Phys Med Rehabil, 1997. **78**(8): p. 808-14.

13. Guest, R.S., et al., *Evaluation of a training program for persons with SCI paraplegia using the Parastep 1 ambulation system: part 4. Effect on physical self-concept and depression.* Arch Phys Med Rehabil, 1997. **78**(8): p. 804-7.

14. Agarwal, S., et al., *Long-term user perceptions of an implanted neuroprosthesis for exercise, standing, and transfers after spinal cord injury.* J Rehabil Res Dev, 2003. **40**(3): p. 241-52.

15. Navarro, X., et al., *A critical review of interfaces with the peripheral nervous system for the control of neuroprostheses and hybrid bionic systems.* J Peripher Nerv Syst, 2005. **10**(3): p. 229-58.

16. Lemay, M.A. and W.M. Grill, *Modularity of motor output evoked by intraspinal microstimulation in cats.* J Neurophysiol, 2004. **91**(1): p. 502-14.

17. Hughes, A.C., L. Guo, and S.P. Deweerth, *Interleaved multichannel epimysial stimulation for eliciting smooth contraction of muscle with reduced fatigue.* Conf Proc IEEE Eng Med Biol Soc, 2010. **1**: p. 6226-9.

18. Singh, K., F.J. Richmond, and G.E. Loeb, *Recruitment properties of intramuscular and nerve-trunk stimulating electrodes.* IEEE Trans Rehabil Eng, 2000. **8**(3): p. 276-85.

19. Triolo, R.J., et al., *Selectivity of intramuscular stimulating electrodes in the lower limbs.* J Rehabil Res Dev, 2001. **38**(5): p. 533-44.

20. Aoyagi, Y., et al., *Movements elicited by electrical stimulation of muscles, nerves, intermediate spinal cord, and spinal roots in anesthetized and decerebrate cats.* IEEE Trans Neural Syst Rehabil Eng, 2004. **12**(1): p. 1-11.

21. Tyler, D.J. and D.M. Durand, *Chronic response of the rat sciatic nerve to the flat interface nerve electrode.* Ann Biomed Eng, 2003. **31**(6): p. 633-42.

22. Veraart, C., W.M. Grill, and J.T. Mortimer, *Selective control of muscle activation with a multipolar nerve cuff electrode.* IEEE Trans Biomed Eng, 1993. **40**(7): p. 640-53.

23. Schiefer, M.A., R.J. Triolo, and D.J. Tyler, *A model of selective activation of the femoral nerve with a flat interface nerve electrode for a lower extremity neuroprosthesis.* IEEE Trans Neural Syst Rehabil Eng, 2008. **16**(2): p. 195-204.

24. Branner, A., R.B. Stein, and R.A. Normann, *Selective stimulation of cat sciatic nerve using an array of varying-length microelectrodes.* J Neurophysiol, 2001. **85**(4): p. 1585-94.

25. McDonnall, D., G.A. Clark, and R.A. Normann, *Interleaved, multisite electrical stimulation of cat sciatic nerve produces fatigue-resistant, ripple-free motor responses.* IEEE Trans Neural Syst Rehabil Eng, 2004. **12**(2): p. 208-15.

26. Bamford, J.A., C.T. Putman, and V.K. Mushahwar, *Intraspinal microstimulation preferentially recruits fatigue-resistant muscle fibres and generates gradual force in rat.* J Physiol, 2005. **569**(Pt 3): p. 873-84.

27. Mushahwar, V.K., D.F. Collins, and A. Prochazka, *Spinal cord microstimulation generates functional limb movements in chronically implanted cats.* Exp Neurol, 2000. **163**(2): p. 422-9.

28. Yakovenko, S., et al., *Spatiotemporal activation of lumbosacral motoneurons in the locomotor step cycle.* J Neurophysiol, 2002. **87**(3): p. 1542-53.

29. Gustafsson, B. and E. Jankowska, *Direct and indirect activation of nerve cells by electrical pulses applied extracellularly.* J Physiol, 1976. **258**(1): p. 33-61.

30. Gaunt, R.A., et al., *Intraspinal microstimulation excites multisegmental sensory afferents at lower stimulus levels than local alpha-motoneuron responses.* J Neurophysiol, 2006. **96**(6): p. 2995-3005.

31. McIntyre, C.C. and W.M. Grill, *Selective microstimulation of central nervous system neurons.* Ann Biomed Eng, 2000. **28**(3): p. 219-33.

32. O'Donovan, M.J., J.A. Hoffer, and G.E. Loeb, *Physiological characterization of motor unit properties in intact cats.* J Neurosci Methods, 1983. **7**(2): p. 137-49.

33. Weber, D.J., et al., *Toward an artificial afferent interface: Closing the somatosensory loop.* IEEE TNSRE, 2010. **in preparation**.

34. Normann, R., D. McDonnall, and G. Clark, *Control of skeletal muscle force with currents injected via an intrafascicular, microelectrode array.* Conf Proc IEEE Eng Med Biol Soc, 2005. **7**: p. 7644-7.

35. Durand, D.M., P. Yoo, and Z. Lertmanorat, *Neural interfacing with the peripheral nervous system.* Conf Proc IEEE Eng Med Biol Soc, 2004. **7**: p. 5329-32.

36. McDonnall, D., G.A. Clark, and R.A. Normann, *Selective motor unit recruitment via intrafascicular multielectrode stimulation.* Can J Physiol Pharmacol, 2004. **82**(8-9): p. 599-609.

37. Goslow, G.E., Jr., R.M. Reinking, and D.G. Stuart, *The cat step cycle: hind limb joint angles and muscle lengths during unrestrained locomotion.* J Morphol, 1973. **141**(1): p. 1-41.

38. Freund, H.J., H.J. Budingen, and V. Dietz, *Activity of single motor units from human forearm muscles during voluntary isometric contractions.* J Neurophysiol, 1975. **38**(4): p. 933-46.

39. Bawa, P., A. Mannard, and R.B. Stein, *Predictions and experimental tests of a visco-elastic muscle model using elastic and inertial loads.* Biol Cybern, 1976. **22**(3): p. 139-45.

40. Bawa, P., A. Mannard, and R.B. Stein, *Effects of elastic loads on the contractions of cat muscles.* Biol Cybern, 1976. **22**(3): p. 129-37.

41. Bawa, P. and R.B. Stein, *Frequency response of human soleus muscle.* J Neurophysiol, 1976. **39**(4): p. 788-93.

42. Baldwin, E.R., P.M. Klakowicz, and D.F. Collins, *Wide-pulse-width, high-frequency neuromuscular stimulation: implications for functional electrical stimulation.* J Appl Physiol, 2006. **101**(1): p. 228-40.

43. Macefield, G., S.C. Gandevia, and D. Burke, *Perceptual responses to microstimulation of single afferents innervating joints, muscles and skin of the human hand.* J Physiol, 1990. **429**: p. 113-29.

44. Moritz, C.T., et al., *Forelimb movements and muscle responses evoked by microstimulation of cervical spinal cord in sedated monkeys.* J Neurophysiol, 2007. **97**(1): p. 110-20.

45. Mushahwar, V.K., et al., *Intraspinal micro stimulation generates locomotor-like and feedback-controlled movements.* IEEE Trans Neural Syst Rehabil Eng, 2002. **10**(1): p. 68-81.

46. Mushahwar, V.K. and K.W. Horch, *Selective activation of muscle groups in the feline hindlimb through electrical microstimulation of the ventral lumbo-sacral spinal cord.* IEEE Trans Rehabil Eng, 2000. **8**(1): p. 11-21.

47. Saigal, R., C. Renzi, and V.K. Mushahwar, *Intraspinal microstimulation generates functional movements after spinal-cord injury.* IEEE Trans Neural Syst Rehabil Eng, 2004. **12**(4): p. 430-40.

48. Namjoshi, D.R., et al., *Network actions of pentobarbital in the rat mesopontine tegmentum on sensory inflow through the spinothalamic tract.* J Neurophysiol, 2009. **102**(2): p. 700-13.

49. Kungys, G., et al., *Propofol produces immobility via action in the ventral horn of the spinal cord by a GABAergic mechanism.* Anesth Analg, 2009. **108**(5): p. 1531-7.

50. Kim, J., et al., *Neurons in the ventral spinal cord are more depressed by isoflurane, halothane, and propofol than are neurons in the dorsal spinal cord.* Anesth Analg, 2007. **105**(4): p. 1020-6, table of contents.

51. Mushahwar, V.K., L. Guevremont, and R. Saigal, *Could cortical signals control intraspinal stimulators? A theoretical evaluation.* IEEE Trans Neural Syst Rehabil Eng, 2006. **14**(2): p. 198-201.

52. Tresch, M.C. and E. Bizzi, *Responses to spinal microstimulation in the chronically spinalized rat and their relationship to spinal systems activated by low threshold cutaneous stimulation.* Exp Brain Res, 1999. **129**(3): p. 401-16.

53. BeMent, S.L. and J.B. Ranck, Jr., *A quantitative study of electrical stimulation of central myelinated fibers.* Exp Neurol, 1969. **24**(2): p. 147-70.

54. Roberts, W.J. and D.O. Smith, *Analysis of threshold currents during microstimulation of fibres in the spinal cord.* Acta Physiol Scand, 1973. **89**(3): p. 384-94.

55. McIntyre, C.C., A.G. Richardson, and W.M. Grill, *Modeling the excitability of mammalian nerve fibers: influence of afterpotentials on the recovery cycle.* J Neurophysiol, 2002. **87**(2): p. 995-1006.

56. Grinberg, Y., et al., *Fascicular perineurium thickness, size, and position affect model predictions of neural excitation.* IEEE Trans Neural Syst Rehabil Eng, 2008. **16**(6): p. 572-81.

57. Murray, K.C., et al., *Motoneuron excitability and muscle spasms are regulated by 5-HT2B and 5-HT2C receptor activity.* J Neurophysiol. **105**(2): p. 731-48.

58. Mushahwar, V.K. and K.W. Horch, *Muscle recruitment through electrical stimulation of the lumbo-sacral spinal cord.* IEEE Trans Rehabil Eng, 2000. **8**(1): p. 22-9.

59. Veltink, P.H., et al., *A modeling study of nerve fascicle stimulation.* IEEE Trans Biomed Eng, 1989. **36**(7): p. 683-92.

60. McNeal, D.R., *Analysis of a model for excitation of myelinated nerve.* IEEE Trans Biomed Eng, 1976. **23**(4): p. 329-37.

61. Tyler, D.J. and D.M. Durand, *Functionally selective peripheral nerve stimulation with a flat interface nerve electrode.* IEEE Trans Neural Syst Rehabil Eng, 2002. **10**(4): p. 294-303.

62. Meier, J.H., et al., *Simulation of multipolar fiber selective neural stimulation using intrafascicular electrodes.* IEEE Trans Biomed Eng, 1992. **39**(2): p. 122-34.

63. Butson, C.R., et al., *Selective neural activation in a histologically derived model of peripheral nerve.* J Neural Eng, 2011. **8**(3): p. 036009.

64. McIntyre, C.C., et al., *Cellular effects of deep brain stimulation: model-based analysis of activation and inhibition.* J Neurophysiol, 2004. **91**(4): p. 1457-69.

65. Butson, C.R. and C.C. McIntyre, *Tissue and electrode capacitance reduce neural activation volumes during deep brain stimulation.* Clin Neurophysiol, 2005. **116**(10): p. 2490-500.

66. Bourbeau, D.J., et al., *A computational model for estimating recruitment of primary afferent fibers by intraneural stimulation in the dorsal root ganglia.* J Neural Eng, 2011. **in press**.

67. Hines, M.L. and N.T. Carnevale, *NEURON: a tool for neuroscientists.* Neuroscientist, 2001. **7**(2): p. 123-35.

68. Risling, M., et al., *Effects of sciatic nerve resection on L7 spinal roots and dorsal root ganglia in adult cats.* Exp Neurol, 1983. **82**(3): p. 568-80.

69. Veale, J.L., R.F. Mark, and S. Rees, *Differential sensitivity of motor and sensory fibres in human ulnar nerve.* J Neurol Neurosurg Psychiatry, 1973. **36**(1): p. 75-86.

70. Panizza, M., et al., *Differences between the time constant of sensory and motor peripheral nerve fibers: further studies and considerations.* Muscle Nerve, 1998. **21**(1): p. 48-54.

71. Panizza, M., et al., *The time constants of motor and sensory peripheral nerve fibers measured with the method of latent addition.* Electroencephalogr Clin Neurophysiol, 1994. **93**(2): p. 147-54.

72. Erlanger, J. and E.A. Blair, *Comparative observations on motor and sensory fibers with special reference to repetitiousness.* American Journal of Physiology, 1938. **121**: p. 431-453.

73. Ranck, J.B., Jr. and S.L. Bement, *The Specific Impedance of the Dorsal Columns of Cat: An Inisotropic Medium.* Exp Neurol, 1965. **11**: p. 451-63.

74. Gaunt, R.A., J.A. Hokanson, and D.J. Weber, *Microstimulation of primary afferent neurons in the L7 dorsal root ganglia using multielectrode arrays in anesthetized cats: thresholds and recruitment properties.* J Neural Eng, 2009. **6**(5): p. 55009.

75. Suh, Y.S., K. Chung, and R.E. Coggeshall, *A study of axonal diameters and areas in lumbosacral roots and nerves in the rat.* J Comp Neurol, 1984. **222**(4): p. 473-81.

76. Boyd, I.A. and K.U. Kalu, *Scaling factor relating conduction velocity and diameter for myelinated afferent nerve fibres in the cat hind limb.* J Physiol, 1979. **289**: p. 277-97.

77. Micera, S. and X. Navarro, *Bidirectional interfaces with the peripheral nervous system.* Int Rev Neurobiol, 2009. **86**: p. 23-38.

78. Li, C.L. and A. Bak, *Excitability characteristics of the A- and C-fibers in a peripheral nerve.* Exp Neurol, 1976. **50**(1): p. 67-79.

79. Milner, T.E., et al., *Improved estimates of conduction velocity distributions using single unit action potentials.* J Neurol Neurosurg Psychiatry, 1981. **44**(6): p. 476-84.

80. Amir, R. and M. Devor, *Electrical excitability of the soma of sensory neurons is required for spike invasion of the soma, but not for through-conduction.* Biophys J, 2003. **84**(4): p. 2181-91.

81. Ranck, J.B., Jr., *Which elements are excited in electrical stimulation of mammalian central nervous system: a review.* Brain Res, 1975. **98**(3): p. 417-40.

82. Lu, H., et al., *Selective extracellular stimulation of individual neurons in ganglia.* J Neural Eng, 2008. **5**(3): p. 287-309.

83. Badia, J., et al., *Topographical distribution of motor fascicles in the sciatic-tibial nerve of the rat.* Muscle Nerve, 2010. **42**(2): p. 192-201.

84. Prodanov, D., N. Nagelkerke, and E. Marani, *Spatial clustering analysis in neuroanatomy: applications of different approaches to motor nerve fiber distribution.* J Neurosci Methods, 2007. **160**(1): p. 93-108.